Jouvenet, N., Neil, S. J., Zhadina, M., Zang, T., Kratovac, Z., Lee, Y., Mcnatt, M., Hatziioannou, T., and Bieniasz, P. D. (2009). Broad-spectrum inhibition of retroviral and filoviral particle release by tetherin. *J. Virol.* 83, 1837–1844.

Kaletsky, R. L., Francica, J. R., Agrawal-Gamse, C., and Bates, P. (2009). Tetherin-mediated restriction of filovirus budding is antagonized by the Ebola glycoprotein. *Proc. Natl. Acad. Sci. U.S.A.* 106, 2886–2891.

Kobayashi, T., Ode, H., Yoshida, T., Sato, K., Gee, P., Yamamoto, S. P., Ebina, H., Strebel, K., Sato, H., and Koyanagi, Y. (2011). Identification of amino acids in the human tetherin transmembrane domain responsible for HIV-1 Vpu interaction and susceptibility. *J. Virol.* 85, 932–945.

Kühl, A., Banning, C., Marzi, A., Votteler, J., Steffen, I., Bertram, S., Glowacka, I., Konrad, A., Stürzl, M., Guo, J.-T., Schubert, U., Feldmann, H., Behrens, G., Schindler, M., and Pöhlmann, S. (2011). The ebola virus glycoprotein and HIV-1 Vpu employ different strategies to counteract the antiviral factor tetherin. *J. Infect. Dis.* 204, S850–S860.

Kupzig, S., Korolchuk, V., Rollason, R., Sugden, A., Wilde, A., and Banting, G. (2003). Bst-2/HM1.24 is a raft-associated apical membrane protein with an unusual topology. *Traffic* 4, 694–709.

Laguette, N., Sobhian, B., Casartelli, N., Ringeard, M., Chable-Bessia, C., Segeral, E., Yatim, A., Emiliani, S., Schwartz, O., and Benkirane, M. (2011). SAMHD1 is the dendritic- and myeloid-cell-specific HIV-1 restriction factor counteracted by Vpx. *Nature* 474, 654–657.

Lau, D., Kwan, W., and Guatelli, J. (2011). Role of the endocytic pathway in the counteraction of BST-2 by human lentiviral pathogens. *J. Virol.* 85, 9834–9846.

Le Tortorec, A., and Neil, S. J. D. (2009). Antagonism to and intracellular sequestration of human tetherin by the human immunodeficiency virus type 2 envelope glycoprotein. *J. Virol.* 83, 11966–11978.

Liberatore, R. A., and Bieniasz, P. D. (2011). Tetherin is a key effector of the antiretroviral activity of type I interferon in vitro and in vivo. *Proc. Natl. Acad. Sci. U.S.A.* 108, 18097–18101.

Lim, E. S., Malik, H. S., and Emerman, M. (2010). Ancient adaptive evolution of tetherin shaped the functions of vpu and nef in human immunodeficiency virus and primate lentiviruses. *J. Virol.* 84, 7124–7134.

Lopez, L. A., Yang, S. J., Hauser, H., Exline, C. M., Haworth, K. G., Oldenburg, J., and Cannon, P. M. (2010). Ebola virus glycoprotein counteracts BST-2/tetherin restriction in a sequence-independent manner that does not require tetherin surface removal. *J. Virol.* 84, 7243–7255.

Malim, M. H., and Emerman, M. (2008). HIV-1 accessory proteins ensuring viral survival in a hostile environment. *Cell Host Microbe* 3, 388–398.

Mangeat, B., Gers-Huber, G., Lehmann, M., Zufferey, M., Luban, J., and Piguet, V. (2009). HIV-1 Vpu neutralizes the antiviral factor tetherin/BST-2 by binding it and directing its beta-TrCP2-dependent degradation. *PLoS Pathog.* 5, e1000574. doi:10.1371/journal.ppat.1000574

Mansouri, M., Viswanathan, K., Douglas, J. L., Hines, J., Gustin, J., Moses, A. V., and Fruh, K. (2009). Molecular mechanism of BST2/tetherin downregulation by K5/MIR2 of Kaposi's sarcoma-associated herpesvirus. *J. Virol.* 83, 9672–9681.

Masuyama, N., Kuronita, T., Tanaka, R., Muto, T., Hirota, Y., Takigawa, A., Fujita, H., Aso, Y., Amano, J., and Tanaka, Y. (2009). HM1.24 is internalized from lipid rafts by clathrin-mediated endocytosis through interaction with α-adaptin. *J. Biol. Chem.* 284, 15927–15941.

McNatt, M. W., Zang, T., Hatziioannou, T., Bartlett, M., Fofana, I. B., Johnson, W. E., Neil, S. J. D., and Bieniasz, P. D. (2009). Species-specific activity of HIV-1 Vpu and positive selection of tetherin transmembrane domain variants. *PLoS Pathog.* 5, e1000300. doi:10.1371/journal.ppat.1000300

Mitchell, R. S., Katsura, C., Skasko, M. A., Fitzpatrick, K., Lau, D., Ruiz, A., Stephens, E. B., Margottin-Goguet, F., Benarous, R., and Guatelli, J. C. (2009). Vpu antagonizes BST-2–mediated restriction of HIV-1 release via β-TrCP and endo-lysosomal trafficking. *PLoS Pathog.* 5, e1000450. doi:10.1371/journal.ppat.1000450

Miyagi, E., Andrew, A. J., Kao, S., and Strebel, K. (2009). Vpu enhances HIV-1 virus release in the absence of Bst-2 cell surface down-modulation and intracellular depletion. *Proc. Natl. Acad. Sci. U.S.A.* 106, 2868–2873.

Moore, R. C., Lee, I. Y., Silverman, G. L., Harrison, P. M., Strome, R., Heinrich, C., Karunaratne, A., Pasternak, S. H., Chishti, M. A., Liang, Y., Mastrangelo, P., Wang, K., Smit, A. F. A., Katamine, S., Carlson, G. A., Cohen, F. E., Prusiner, S. B., Melton, D. W., Tremblay, P., Hood, L. E., and Westaway, D. (1999). Ataxia in prion protein (PrP)-deficient mice is associated with upregulation of the novel PrP-like protein doppel. *J. Mol. Biol.* 292, 797–817.

Neil, S. J., Zang, T., and Bieniasz, P. D. (2008). Tetherin inhibits retrovirus release and is antagonized by HIV-1 Vpu. *Nature* 451, 425–430.

Ohtomo, T., Sugamata, Y., Ozaki, Y., Ono, K., Yoshimura, Y., Kawai, S., Koishihara, Y., Ozaki, S., Kosaka, M., Hirano, T., and Tsuchiya, M. (1999). Molecular cloning and characterization of a surface antigen preferentially overexpressed on multiple myeloma cells. *Biochem. Biophys. Res. Commun.* 258, 583–591.

Pais-Correia, A.-M., Sachse, M., Guadagnini, S., Robbiati, V., Lasserre, R., Gessain, A., Gout, O., Alcover, A., and Thoulouze, M.-I. (2010). Biofilm-like extracellular viral assemblies mediate HTLV-1 cell-to-cell transmission at virological synapses. *Nat. Med.* 16, 83–89.

Panchal, R. G., Ruthel, G., Kenny, T. A., Kallstrom, G. H., Lane, D., Badie, S. S., Li, L., Bavari, S., and Aman, M. J. (2003). In vivo oligomerization and raft localization of Ebola virus protein VP40 during vesicular budding. *Proc. Natl. Acad. Sci. U.S.A.* 100, 15936–15941.

Pardieu, C., Vigan, R., Wilson, S. J., Calvi, A., Zang, T., Bieniasz, P., Kellam, P., Towers, G. J., and Neil, S. J. D. (2010). The RING-CH ligase K5 antagonizes restriction of KSHV and HIV-1 particle release by mediating ubiquitin-dependent endosomal degradation of tetherin. *PLoS Pathog.* 6, e1000843. doi:10.1371/journal.ppat.1000843

Perez-Caballero, D., Zang, T., Ebrahimi, A., Mcnatt, M. W., Gregory, D. A., Johnson, M. C., and Bieniasz, P. D. (2009). Tetherin inhibits HIV-1 release by directly tethering virions to cells. *Cell* 139, 499–511.

Radoshitzky, S. R., Dong, L., Chi, X., Clester, J. C., Retterer, C., Spurgers, K., Kuhn, J. H., Sandwick, S., Ruthel, G., Kota, K., Boltz, D., Warren, T., Kranzusch, P. J., Whelan, S. P., and Bavari, S. (2010). Infectious Lassa virus, but not filoviruses, is restricted by BST-2/tetherin. *J. Virol.* 84, 10569–10580.

Ritter, G. D. Jr., Yamshchikov, G., Cohen, S. J., and Mulligan, M. J. (1996). Human immunodeficiency virus type 2 glycoprotein enhancement of particle budding: role of the cytoplasmic domain. *J. Virol.* 70, 2669–2673.

Rollason, R., Korolchuk, V., Hamilton, C., Jepson, M., and Banting, G. (2009). A CD317/tetherin–RICH2 complex plays a critical role in the organization of the subapical actin cytoskeleton in polarized epithelial cells. *J. Cell Biol.* 184, 721–736.

Rollason, R., Korolchuk, V., Hamilton, C., Schu, P., and Banting, G. (2007). Clathrin-mediated endocytosis of a lipid-raft-associated protein is mediated through a dual tyrosine motif. *J. Cell. Sci.* 120, 3850–3858.

Rong, L., Zhang, J., Lu, J., Pan, Q., Lorgeoux, R.-P., Aloysius, C., Guo, F., Liu, S.-L., Wainberg, M. A., and Liang, C. (2009). The transmembrane domain of BST-2 determines its sensitivity to down-modulation by human immunodeficiency virus type 1 Vpu. *J. Virol.* 83, 7536–7546.

Ruiz, A., Hill, M. S., Schmitt, K., and Stephens, E. B. (2010). Membrane raft association of the Vpu protein of human immunodeficiency virus type 1 correlates with enhanced virus release. *Virology* 408, 89–102.

Sakuma, T., Noda, T., Urata, S., Kawaoka, Y., and Yasuda, J. (2009a). Inhibition of Lassa and Marburg virus production by tetherin. *J. Virol.* 83, 2382–2385.

Sakuma, T., Sakurai, A., and Yasuda, J. (2009b). Dimerization of tetherin is not essential for its antiviral activity against Lassa and Marburg viruses. *PLoS ONE* 4, e6934. doi:10.1371/journal.pone.0006934

Sauter, D., Schindler, M., Specht, A., Landford, W. N., Münch, J., Kim, K.-A., Votteler, J., Schubert, U., Bibollet-Ruche, F., Keele, B. F., Takehisa, J., Ogando, Y., Ochsenbauer, C., Kappes, J. C., Ayouba, A., Peeters, M., Learn, G. H., Shaw, G., Sharp, P. M., Bieniasz, P., Hahn, B. H., Hatziioannou, T., and Kirchhoff, F. (2009). Tetherin-driven adaptation of Vpu and Nef function and the evolution of pandemic and nonpandemic HIV-1 strains. *Cell Host Microbe* 6, 409–421.

Schubert, H. L., Zhai, Q., Sandrin, V., Eckert, D. M., Garcia-Maya, M., Saul, L., Sundquist, W. I., Steiner, R. A., and Hill, C. P. (2010). Structural and functional studies on the extracellular domain of BST2/tetherin in reduced and oxidized conformations. *Proc. Natl. Acad. Sci. U.S.A.* 107, 17951–17956.

Schubert, U., and Strebel, K. (1994). Differential activities of the human immunodeficiency virus type 1-encoded Vpu protein are regulated by phosphorylation and occur in different cellular compartments. *J. Virol.* 68, 2260–2271.

Sheehy, A. M., Gaddis, N. C., Choi, J. D., and Malim, M. H. (2002). Isolation of a human gene that inhibits HIV-1 infection and is suppressed by the viral Vif protein. *Nature* 418, 646–650.

Shingai, M., Yoshida, T., Martin, M. A., and Strebel, K. (2011). Some human immunodeficiency virus type 1 Vpu proteins are able to antagonize macaque BST-2 in vitro and in vivo: Vpu-negative simian-human immunodeficiency viruses are attenuated in vivo. *J. Virol.* 85, 9708–9715.

Skasko, M., Tokarev, A., Chen, C.-C., Fischer, W. B., Pillai, S. K., and Guatelli, J. (2011a). BST-2 is rapidly down-regulated from the cell surface by the HIV-1 protein Vpu: evidence for a post-ER mechanism of Vpu-action. *Virology* 411, 65–77.

Skasko, M., Wang, Y., Tian, Y., Tokarev, A., Munguia, J., Ruiz, A., Stephens, E. B., Opella, S. J., and Guatelli, J. (2011b). HIV-1 Vpu antagonizes the innate restriction factor BST-2 via lipid-embedded helix-helix interactions. *J. Biol. Chem.* doi: 10.1074/jbc.M111.296772. [Epub ahead of print].

Strebel, K., Klimkait, T., and Martin, M. A. (1988). A novel gene of HIV-1, vpu, and its 16-kilodalton product. *Science* 241, 1221–1223.

Stremlau, M., Owens, C. M., Perron, M. J., Kiessling, M., Autissier, P., and Sodroski, J. (2004). The cytoplasmic body component TRIM5alpha restricts HIV-1 infection in old world monkeys. *Nature* 427, 848–853.

Swiecki, M., Scheaffer, S. M., Allaire, M., Fremont, D. H., Colonna, M., and Brett, T. J. (2011). Structural and biophysical analysis of BST-2/tetherin ectodomains reveals an evolutionary conserved design to inhibit virus release. *J. Biol. Chem.* 286, 2987–2997.

Tokarev, A. A., Munguia, J., and Guatelli, J. C. (2011). Serine-threonine ubiquitination mediates downregulation of BST-2/tetherin and relief of restricted virion release by HIV-1 Vpu. *J. Virol.* 85, 51–63.

Van Damme, N., Goff, D., Katsura, C., Jorgenson, R. L., Mitchell, R., Johnson, M. C., Stephens, E. B., and Guatelli, J. (2008). The interferon-induced protein BST-2 restricts HIV-1 release and is downregulated from the cell surface by the viral Vpu protein. *Cell Host Microbe* 3, 245–252.

Vigan, R., and Neil, S. J. D. (2010). Determinants of tetherin antagonism in the transmembrane domain of the human immunodeficiency virus type 1 Vpu protein. *J. Virol.* 84, 12958–12970.

Waheed, A. A., and Freed, E. O. (2009). Lipids and membrane microdomains in HIV-1 replication. *Virus Res.* 143, 162–176.

Watanabe, R., Leser, G. P., and Lamb, R. A. (2011). Influenza virus is not restricted by tetherin whereas influenza VLP production is restricted by tetherin. *Virology* 417, 50–56.

Weidner, J. M., Jiang, D., Pan, X. B., Chang, J., Block, T. M., and Guo, J. T. (2010). Interferon-induced cell membrane proteins, IFITM3 and tetherin, inhibit vesicular stomatitis virus infection via distinct mechanisms. *J. Virol.* 84, 12646–12657.

Xu, F., Tan, J., Liu, R., Xu, D., Li, Y., Geng, Y., Liang, C., and Qiao, W. (2011). Tetherin inhibits prototypic foamy virus release. *Virol. J.* 8, 198.

Yang, H., Wang, J., Jia, X., Mcnatt, M. W., Zang, T., Pan, B., Meng, W., Wang, H.-W., Bieniasz, P. D., and Xiong, Y. (2010a). Structural insight into the mechanisms of enveloped virus tethering by tetherin. *Proc. Natl. Acad. Sci. U.S.A.* 107, 18428–18432.

Yang, S. J., Lopez, L. A., Hauser, H., Exline, C. M., Haworth, K. G., and Cannon, P. M. (2010b). Anti-tetherin activities in Vpu-expressing primate lentiviruses. *Retrovirology* 7, 13.

Yoshida, T., Kao, S., and Strebel, K. (2011). Identification of residues in the BST-2 TM domain important for antagonism by HIV-1 Vpu using a gain-of-function approach. *Front. Microbiol.* 2:35. doi:10.3389/fmicb.2011.00035

Zhang, F., Wilson, S. J., Landford, W. C., Virgen, B., Gregory, D., Johnson, M. C., Munch, J., Kirchhoff, F., Bieniasz, P. D., and Hatziioannou, T. (2009). Nef proteins from simian immunodeficiency viruses are tetherin antagonists. *Cell Host Microbe* 6, 54–67.

Conflict of Interest Statement: The authors declare that the research was conducted in the absence of any commercial or financial relationships that could be construed as a potential conflict of interest.

Received: 18 November 2011; accepted: 25 November 2011; published online: 12 December 2011.

Citation: Arias JF, Iwabu Y and Tokunaga K (2011) Structural basis for the antiviral activity of BST-2/tetherin and its viral antagonism. Front. Microbio. 2:250. doi: 10.3389/fmicb.2011.00250

This article was submitted to Frontiers in Virology, a specialty of Frontiers in Microbiology.

J Neuroimmune Pharmacol (2011) 6:177–187
DOI 10.1007/s11481-011-9276-5

BRIEF REPORT

Identification of SNF2h, a Chromatin-Remodeling Factor, as a Novel Binding Protein of Vpr of Human Immunodeficiency Virus Type 1

Daiki Taneichi · Kenta Iijima · Akihiro Doi · Takayoshi Koyama · Yuzuru Minemoto · Kenzo Tokunaga · Mari Shimura · Shigeyuki Kano · Yukihito Ishizaka

Received: 10 November 2010 / Accepted: 16 March 2011 / Published online: 26 April 2011

Abstract *Vpr*, an accessory gene of human immunodeficiency virus type 1, encodes a virion-associated nuclear protein that plays an important role in the primary viral infection of resting macrophages. It has a variety of biological functions, including roles in a cell cycle abnormality at G_2/M phase, apoptosis, nuclear transfer of preintegration complex, and DNA double-strand breaks (DSBs), some of which depend on its association with the chromatin of the host cells. Given that DSB signals are postulated to be a positive factor in the viral infection, understanding the mode of chromatin recruitment of Vpr is important. Here, we identified SNF2h, a chromatin-remodeling factor, as a novel binding partner of Vpr involved in its chromatin recruitment. When endogenous SNF2h protein was extensively downregulated by *SNF2h* small interfering RNA (siRNA), the amount of Vpr loaded on chromatin decreased to about 30% of the control level. Biochemical analysis using a mutant Vpr suggested that Vpr binds SNF2h via HFRIG (amino acids 71–75 depicted by single letters) and the Vpr mutant lacking this motif lost the activity to induce DSB-dependent signals. Consistently, Vpr-induced DSBs were attenuated by extensive downregulaion of endogenous *SNF2h*. Based on these data, we discuss the role of DSB and DSB signals in the viral infection.

Keywords HIV-1 · Vpr · SNF2h · Chromatin recruitment · DNA damage signal

Daiki Taneichi and Kenta Iijima contributed equally to this work.

Electronic supplementary material The online version of this article (doi:10.1007/s11481-011-9276-5) contains supplementary material, which is available to authorized users.

D. Taneichi · K. Iijima · A. Doi · T. Koyama · Y. Minemoto · M. Shimura · Y. Ishizaka (✉)
Department of Intractable Diseases,
National Center for Global Health and Medicine,
1-21-1 Toyama,
Shinjuku, Tokyo 162-8655, Japan
e-mail: zakay@ri.ncgm.go.jp

D. Taneichi · S. Kano
Graduate School of Comprehensive Human Sciences,
University of Tsukuba,
1-1-1 Ten-nodai,
Tsukuba 305-8577, Japan

K. Tokunaga
Department of Pathology, National Institute of Infectious Diseases,
1-23-1 Toyama,
Shinjuku, Tokyo 162-8640, Japan

S. Kano
Department of Tropical Medicine and Malaria, Research Institute,
National Center for Global Health and Medicine,
Tokyo 162-8655, Japan
e-mail: kano@ri.ncgm.go.jp

Introduction

Highly active antiretroviral therapy (HAART) has improved the prognosis of human immunodeficiency virus type 1 (HIV-1)-positive patients, but the complete eradication of the virus from infected patients is difficult due to the presence of latent viral reservoirs (Wong et al. 1997). Notably, even with HAART, the virus is thought to be produced from infected macrophages, a latent viral reservoir (Finzi et al. 1997),

suggesting that clarifying the mechanism of viral infection of resting macrophages is important. *Vpr*, an accessory gene of HIV-1, encodes a virion-associated 14-kDa protein involved in the primary infection into resting macrophages (Heinzinger et al. 1994; Vodicka et al. 1998). As striking evidence of this, studies on experimental animal models and an infected human revealed that the virus with wild-type Vpr spreads in vivo, indicating that Vpr confers a replication advantage on the virus in vivo (Goh et al. 1998).

Vpr has a variety of biological functions including roles in a cell cycle perturbation at G_2/M phase, the induction of the ATR-dependent DNA damage response and apoptosis (see a review by Andersen et al. 2008). In addition to ATR activation, we reported that viral infection induced DNA double-strand breaks (DSBs; Tachiwana et al. 2006) and identified that Vpr was responsible for DSBs (Shimura et al. 1999a, b; Nakai-Murakami et al. 2007). Since KU55933, an ATM inhibitor, inhibits the viral infection (Lau et al. 2005), DSBs or DSB signals induced by Vpr may be positively involved in the viral infection. Because DSB signals were proposed to depend on the chromatin recruitment of Vpr (Lai et al. 2005), determining its molecular mechanism is imperative. Consistent with a report that an HFRIG motif encompassing amino acids 71–75 was required for the chromatin recruitment of Vpr (Lai et al. 2005), we recently reported that a Vpr mutant lacking this motif is not present in the chromatin fraction and never induced ATM- or ATR-dependent cellular signals (Nakai-Murakami et al. 2009). These data support the idea that the motif is involved in the molecular interaction of Vpr with uncharacterized cellular protein(s) required for the chromatin recruitment of Vpr.

SNF2h, a member of SWI/SNF, is ATP-dependent chromatin-remodeling factor. Members of the SWI/SNF family are involved in the functional modification of nucleosomes: changing of nucleosome positions, loading of genomic DNA loop to nucleosome, and exchanging histone octomers (Racki and Narlikar 2008). Depending on binding partners, SNF2h is involved in a variety of biological functions related to packaging or relaxing the chromatin structure of the genome during DNA replication, transcription, repair, and recombination (Lusser and Kadonaga. 2003). Recently, SNF2h was also shown to be involved in the formation of a higher-order structure of chromatin by functioning as a loading factor for hRAD21 (Hakimi et al. 2002) and CENP-A (Izuta et al. 2006) to chromatin. In addition, SNF2h is involved in DNA replication in the centromeric region during late S-phase (Poot et al. 2004). Without SNF2h, ACF1, a counterpart of SNF2h, is not loaded on the centromere, and DNA replication at the corresponding region is not provoked. Data suggested that unpacking of the chromatin structure, which is regulated cooperatively by SNF2h and ACF1, must be coordinated with DNA replication; otherwise, DNA replication at the corresponding region is delayed.

Here, we identified cellular factors responsible for the chromatin recruitment of Vpr. Several studies identified numbers of Vpr-associating molecules (Andersen et al. 2008), and we here adopted a novel approach, a random peptide display library (RPDL) using a recombinant Vpr (rVpr) as bait. First, we identified a peptide with an affinity for rVpr (Vpr-associating peptide-1, VAP-1), and a polyclonal antibody was raised against VAP-1. Then, cellular molecules were identified by immunoprecipitation (IP) followed by time-of-flight/mass spectrometry (TOF–MS) analysis. We identified SNF2h as a novel binding partner. Based on results supporting direct binding of SNF2h and rVpr, and DSBs under the downregulated expression of endogenous SNF2h, we discuss the mechanism of Vpr-induced DSBs and their roles in viral infection.

Materials and methods

Cell culture and treatment

HEK293T cells (a human embryonic kidney cell line) and HeLa cells (a human cervical carcinoma cell line, RCB0007) were from RIKEN BioResource Center Cell Bank. TIG-3 cells (primary human fibroblast cells) were from the Health Science Research Resources Bank (Osaka, Japan); 2008 cells (a human ovary carcinoma cell line) were a kind gift from Dr. Hiroshi Sasaki (Jikei Medical School). MIT-23 cell line is derived from HT1080 cells, in which Vpr expression is controlled by a tetracycline-responsive promoter, as previously described (Shimura et al. 1999a). Cells were maintained at 37°C in 5% CO_2 in Dulbecco's modified Eagle's medium (DMEM) supplemented with 10% fetal bovine serum (FBS; Sigma). siRNA oligonucleotides (Invitrogen or Ambion) were transfected using Lipofectamine 2000 or Lipofectamine RNAiMAX reagent (Invitrogen). Sequences of oligonucleotides used for *SNF2h* knockdown are 5′<uaauccucggaccugauaaaucucuc>3′ and 5′<gagagauuaucagguccgaggauua>3′ (#10620312, Invitrogen), 5′<ggagauacuuaguaauagatt>3′ and 5′<ucuauuacu aaguaucuccaa>3′ (s16081, Ambion), and 5′<gggcgaaaguuca cuuagatt>3′ and 5′<ucuaagugaacuuucgcccat>3′ (s16083, Ambion) as sense and antisense primer, respectively. As control, Silencer Negative Control siRNA #2 (Cat# AM4637 Applied Biosystems) was used.

Antibodies

The αVAP-1 rabbit polyclonal antibodies were raised by Nippon Biotest Laboratory (Hachioji, Japan) using a synthetic

VAP-1: CRSSGHSRNQLGV peptide (IBL, Takasaki, Japan). Antibodies against Vpr [8D1] (Hoshino et al. 2007), SNF2h (Abcam), phospho-ATM (Ser 1981) (α-pATM) and phospho-Histone H2AX (Ser139; α–γH2AX; FITC-conjugated; Millipore), GAPDH (Trevigen), HH3 (Millipore), Flag M2 (Sigma), and GFP (MBL) were used as first antibodies. Antibodies against mouse IgG (GE Healthcare), rabbit IgG (GE Healthcare), and goat IgG (Santa Cruz Biotechnology) conjugated with horseradish peroxidase were used as second antibodies.

Plasmids

Vpr was amplified by PCR and subcloned in-frame into the *Bam*HI and *Not*I sites of the pFLAG-CMV-2 vector (Sigma). To create EGFP-Vpr expression plasmid pCA-EGFP-Vpr, Vpr was amplified by PCR and subcloned in-frame into the *Xho*I and *Not*I sites and EGFP into *Kpn*I and *Xho*I site of the pCA vector (Niwa et al. 1996).

Identification of SNF2h as a binding partner of Vpr

Cells were collected, washed with phosphate-buffered saline pH 7.4 (PBS), and resuspended in 500 μL of solution A (10 mM HEPES (pH 7.9), 10 mM KCl, 1.5 mM $MgCl_2$, 0.34 M sucrose, 10% glycerol, 1 mM DTT, 10 mM NaF, 1 mM Na_2VO_3, protease inhibitors) with 0.5% Triton X-100. Cells were incubated on ice for 5 min followed by centrifugation (1,300×*g*, 5 min) to separate cytoplasmic proteins from nuclei (cytosol fraction). Isolated nuclei were then washed twice with solution A and lysis in buffer (50 mM Tris HCl (pH 8.0), 150 mM NaCl, 1 mM EDTA, 0.1% sodium dodecyl sulfate (SDS), 0.5% sodium deoxycholate, 1% NP-40, protease inhibitors (Roche)). Nuclear extracts were immunoprecipitated with αVAP-1 and were analyzed by SDS–polyacrylamide gel electrophoresis (PAGE), and protein was detected by silver staining. Among molecules precipitated with αVAP-1, a protein with molecular weight of about 130 kDa was abolished by the preincubation of the VAP-1 peptide in both cell lines. The 130-kDa band was analyzed by micro-mass Q TOF Ultima (Gene World, Tokyo, Japan). Homology search by the MASCOT-soft program (MASCOT score 504, coverage 9%) revealed that SNF2h was a predominant candidate cellular molecule.

For pull-down experiments, isolated nuclei were washed twice with solution A and resuspended in solution B (3 mM EDTA, 0.2 mM EGTA, 1 mM DTT, and protease inhibitors). After incubation on ice for 10 min, soluble nuclear proteins were prepared from insoluble chromatin fraction by centrifugation (1,700×*g*, 5 min). After washing twice with solution C (10 mM Tris HCl (pH 8.0), 150 mM NaCl, 1 mM EDTA, and 1% NP-40), the recovered pellet was resuspended in 300 μL solution C that contained 1.5 mM $MgCl_2$ and 300 U Benzonase (Novagen). Cells were incubated on ice 30 min followed by centrifugation (10,000×*g*, 20 min), and the supernatant was used as chromatin-enriched fraction.

To show direct binding of Vpr and SNF2h, each recombinant protein was first prepared. Vpr was amplified by PCR and subcloned in-frame into the *Bam*HI and *Not*I sites of the pGEX6-P-1 expression vector (Hoshino et al. 2010). An rVpr-fused GST was expressed and purified, according to the manufacturer's protocol (GE Healthcare). *SNF2h* cDNA was amplified by PCR and subcloned in-frame into the *Bam*HI and *Kpn*I sites of the pFastBac HTb baculovirus expression vector. A His6-tagged rSNF2h was expressed and purified, according to the manufacturer's protocol (GibcoBRL). Five micrograms of rVpr was mixed with 5 μg of a $(His)_6$ tagged-rSNF2h protein conjugated on 40 μL of Ni-NTA agarose (Invitrogen), pre-incubated at 4°C in 200 μL of binding buffer (10 mM Tris–HCl pH 8.0, 150 mM NaCl, 1 mM EDTA, 0.1% NP-40). The binding reaction was allowed to proceed for 1 h at 4°C. After extensive washing with the binding buffer, the beads were resuspended in 50 μL of SDS loading buffer and subject to SDS–PAGE. The proteins were detected by Western blot.

Flow cytometry

Cells were stained with α–γH2AX and analyzed, according to the reported procedures (Porcedda et al. 2008) with minor modifications. Cells were collected, fixed in cold 70% ethanol, and stored at −20°C for up to 2 weeks before analysis. Cells were washed in PBS(+) and then rehydrated for 10 min at 4°C in PBS(+) containing 4% FBS and 0.1% Triton X-100 (PST) (Sigma-Aldrich) prior to staining with FITC-conjugated α–γH2AX mAb diluted 1:400 in PST and incubated for 1.5 h at room temperature. Next, they were washed with PST, and their phase in the cell cycle was determined from their DNA content. Briefly, cells were treated with 500 μg/mL RNase A and 1 μg/mL propidium iodide (PI; Sigma-Aldrich) and incubated for 0.5 h at room temperature. A minimum of 10,000 stained cells were acquired on a FACScan (Becton Dickinson) and analyzed with the CellQuest software.

Immunostaining

The cells were washed with PBS and fixed with 2% paraformaldehyde in PBS. The fixed cells were permeabilized with 0.5% Triton X-100 in PBS for 5 min. After treatment with PBS and 10% goat serum for 30 min, the cells were incubated with α-pATM. After 1 h of incubation at 37°C, secondary antibodies conjugated with Alexa 546 (Molecular Probes) were added for 1 h at 37°C. Nuclei

were stained by Hoechst33258. The slides were mounted in an anti-fade solution (KPL) and analyzed by fluorescence microscopy (Olympus).

Effects of SNF2h siRNA on rVpr-induced DSBs

MIT-23 cells or TIG-3 cells were first transfected with *SNF2h* or control siRNAs using Lipofectamine 2000. On the next day, MIT-23 cells were added with 2.5 μg/mL of doxycycline (DOX) and subjected to immunohistochemical analysis and cell cycle analysis 2 days later. TIG-3 cells were placed under serum-starved conditions (0.1% FBS/DMEM) for 24 h and then treated for additional 24 h with rVpr (50-100 ng/mL) and subjected to an immunohistochemical analysis. Cell cycle arrest of TIG-3 cells after culture for single day in 0.1% FBS/DMEM was confirmed by the bromodeoxyuridine incorporation (Sigma; Koyama, data not shown). rVpr was prepared, as described (Hoshino et al. 2010). To reduce endogenous protein of TIG-3 cells to a maximum level, second transfection of each siRNA (100 nM) was performed with Lipofectamine RNAiMAX reagent 24 h after the initial transfection. After 12 h of second transfection, cells were added with rVpr. Then, an immunohistochemical analysis and neutral Comet assay were carried out after 24 h.

Neutral comet assay (single cell gel electrophoresis)

Neutral Comet assay (Fairbairn et al. 1995) was performed according to manufacturer's protocol (Trevigen) with minor modifications. Briefly, TIG-3 cells were dispersed by pre-warmed Accutase (Innovative cell technologies Inc.) and collected by five volumes of PBS(−) supplemented with 10% FBS, followed by washing with TNE buffer (10 mM Tris–HCl (pH 7.5), 100 mM NaCl, 1 mM EDTA). The cell pellets were suspended in TNE buffer at the concentration of 5×10^5 cells/mL. Two thousands cells were mixed with low melting point agarose and spread on Comet slide (Trevigen), followed by treatment with lysis solution (Trevigen) and incubated with neutral electrophoresis buffer (100 mM Tris-Ac, 300 mM sodium acetate (pH 9.0)). Electrophoresis was performed at 0.75 V/cm for 20 min in pre-chilled neutral electrophoresis buffer under cool condition. After treatment with precipitation buffer (85% ethanol containing 1 M NH_4Ac) followed by 70% ethanol, the slides were completely dried up and stained with SYBR Green solution (Molecular probes). The images were obtained by fluorescence microscopy (Olympus). Comet analysis was performed with CASP software (http://www.casp.of.pl), and Olive tail moment was used as a parameter to quantify the amounts of DSBs. In each treatment, at least 50 cells were analyzed, and more than three independent experiments were performed.

Results

Preparation of a recombinant Vpr protein and identification of VAP-1, a novel peptide with affinity to Vpr

To express rVpr, we used *Pichia pastoris*, a yeast expression system. A DNA fragment of *Vpr* was first amplified from pBabe-vpr (He et al. 1995), and cloned into the pPICZαC (pPICZ-vpr). SMD1168 cells, a strain of *P. pastoris*, were introduced with pPICZ-vpr, and transfectants were selected on YPD plates in the presence of 100 μg/mL of Zeocin. Each selected clone was further cultured in a medium for checking the protein expression. As shown in Fig. 1a, three out of 12 clones were positive for rVpr with about 15 kDa in size in the culture supernatant (indicated by arrow). Using several litters of clone 10 (lane 11), we prepared a purified rVpr by using two steps of purification procedures: ammonium precipitation and phenyl-sepharose column chromatography (Fig. 1b).

To obtain information about a peptide with affinity to rVpr, we screened peptide(s) using RPDL with the purified rVpr as a bait (Frulloni et al. 2009). The RPDL used in the current study was based on a FliTrx system, in which randomly aligned 12-mer amino acids were expressed as parts of bacteria flagellin proteins. We repeated five times of panning followed by amplification of Vpr-bound bacteria and cloned after the last panning and amplification. Then, plasmid DNA in each bacterium was purified and sequence analysis was done. Surprisingly, out of 16 clones analyzed, seven clones had completely the same nucleotide sequence that would encode RSSGHSRNGLG (amino acids depicted by single letters; Fig. 1c). Additionally, a motif of RSSG-----G was detected in additional one clone (Fig. 1c, clone no. 8, "-" depicts different amino acids). Data strongly suggested that some motif(s) present in these eight clones had a high binding affinity to rVpr and we named VAP-1 on a peptide of RSSGHSRNGLG.

Using a synthesized VAP-1 peptide as an immunogen, we generated a polyclonal antibody. To identify candidate molecules, chromatin fractions of two human cell lines, 2008 cells and HeLa cells, were immunoprecipitated with αVAP-1 and were analyzed by SDS–PAGE. Among molecules precipitated with αVAP-1, a protein with molecular weight of about 130 kDa disappeared by the preincubation with the VAP-1 peptide (Fig. 1d, arrow) in both cell lines. We hypothesized that the detected band was a candidate molecule. The polyacrylamide gel corresponding to the 130-kDa protein was excised and subjected to analysis of TOF–MS analysis. Homology search by the MASCOT-soft program (MASCOT score 504, coverage 9%) revealed that SNF2h was a predominant candidate cellular molecule present in the band.

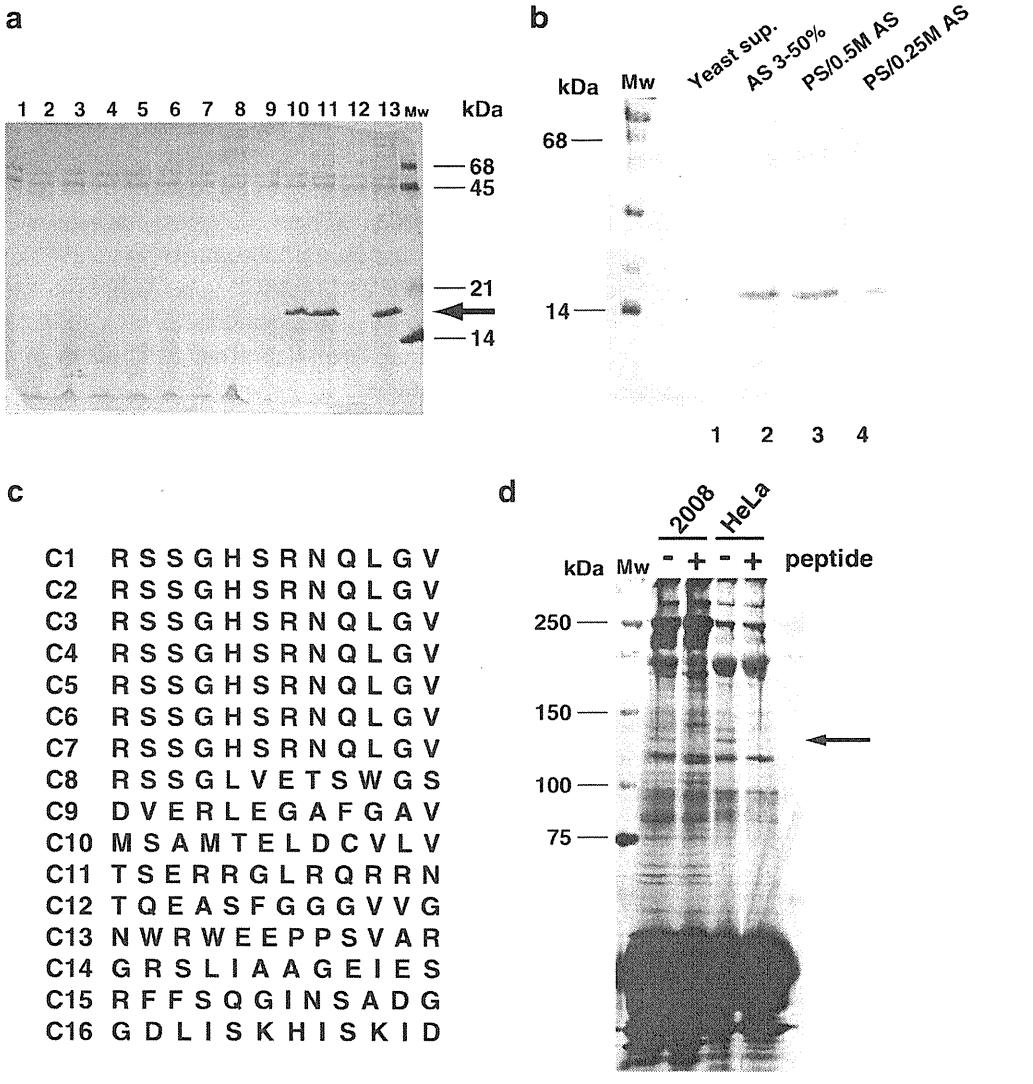

Fig. 1 Identification of VAP-1. **a** SMD1168 cells were introduced with pPICZ-Vpr and selected on YPD plates in the presence of 100 μg/mL Zeocin. Staining with Coomassie brilliant blue (CBB) after SDS–PAGE identified three clones positive for rVpr. *Arrow* indicates the position of the expressed rVpr. *Lane 1*, culture supernatant of control SMD1168 cells; *lanes 2–13*, Zeocin-resistant clones. *Mw* molecular weight marker. **b** Purification of rVpr. rVpr was purified by a phenyl-sepharose column chromatography. *AS* ammonium sulfate, *PS* phenyl-sepharose. Purity was checked by CBB staining after SDS–PAGE. WB using a monoclonal antibody detected the purified protein (Ishizaka Y., data not shown). **c** Alignment of deduced amino acids of 16 independent clones obtained from RPDL. Amino acids were described by *single letters*. Of note, clones (C) 1–7 had similar sequences and C8 contained a common amino acid sequence with C1–7. **d** Identification of candidate cellular protein related to VAP-1. Cell extracts of human 2008 cells and HeLa cells were immunoprecipitated with αVAP-1 without or with VAP-1. *Arrow* indicates the position of the peptide detected by αVAP-1, which was blocked by the addition of excess amount of VAP-1. Proteins were detected by silver staining

SNF2h as a novel binding partner of Vpr

To confirm that SNF2h was an authentic binding protein of Vpr, we first performed a fractionation analysis and observed that similar to Vpr, SNF2h was present in the chromatin fraction (Fig. 2a, lane 3). Additionally, SNF2h was recovered by an IP with αVAP-1 (Fig. 2b, lane 3, arrow). To examine the interaction of Vpr with SNF2h within cells, IP followed by WB was carried out on the cell extracts prepared from transfectants that had been introduced with a plasmid DNA encoding Vpr. As shown in Fig. 2c (lane 2), the precipitate recovered with 8D1 contained SNF2h. Conversely, the precipitate recovered by αSNF2h was also positive for Vpr.

The direct molecular interaction of Vpr and SNF2h was further examined using recombinant proteins of $(His)_6$-SNF2h and GST-Vpr. As shown in Fig. 2d, wild-type (WT) Vpr directly bound SNF2h. In striking contrast, the Vpr mutant lacking amino acids 71–75 (Δ71–75) did not interact with SNF2h (Fig. 2d). These data clearly indicated that SNF2h is a novel binding partner that directly binds Vpr, the interaction of which was dependent on amino acids Δ71–

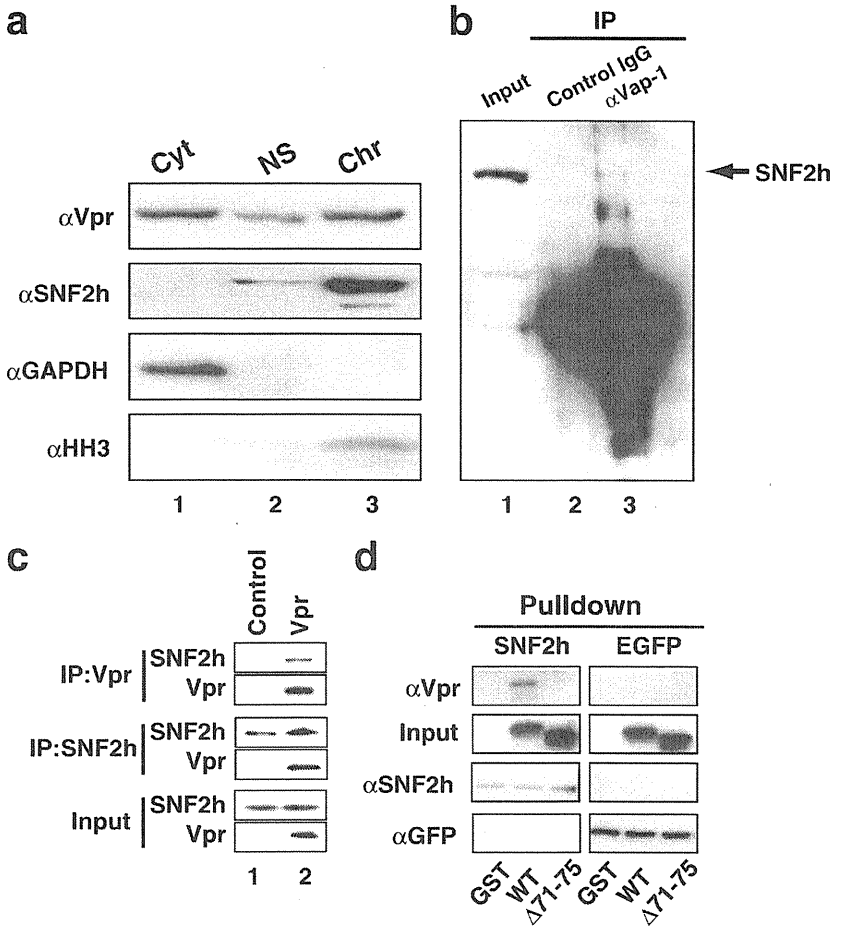

Fig. 2 SNF2h is a novel binding protein of Vpr. **a** Sub-cellular fractionation of SNF2h. HEK293T cells were transfected with pCMV-Vpr. Then, cytosolic, nuclear soluble, and nuclear insoluble (chromatin) fractions were prepared and subjected to Western blot analysis. As control, GAPDH and HH3 were included. *Lane 1* cytosol fraction (*Cyt*), *lane 2* nuclear soluble fraction (*NS*), *lane 3* chromatin fraction (*Chr*). **b** SNF2h is immunoprecipitated by αVAP-1. Nuclear extract of HEK293T cells was immunoprecipitated with αVAP-1, and then WB was carried out with αSNF2h. *Lane 1* a recombinant protein of SNF2h, *lane 2* IP with control IgG, *lane 3* IP with αVAP-1. **c** Molecular interaction of Vpr and SNF2h in vivo. HEK293T cells were transfected with pCMV-Vpr, and IP followed by WB was carried out. As "Input" sample, about one tenth of each original extract was applied. *Lane 1* vector control, *lane 2* pCMV-Vpr. **d** Direct association of WT Vpr and SNF2h. WT and Δ71–75 mutant Vpr proteins were mixed with $(His)_6$-SNF2h or $(His)_6$-EGFP and recovered with Ni-NTA agarose beads and subjected to WB. $(His)_6$-EGFP was included as control

75 of Vpr. VAP-1 has an amino acid stretch composed of RNQLG, a destruction (D)-box motif (RXXL) present in cyclins (Glotzer et al. 1991). It has been well analyzed that D-box present in cyclin B1 is involved in the ubiquitin-dependent degradation of the molecule during cell cycle transition from G_2 phase to M phase (van Zon et al. 2010). SNF2h has four copies of the D-box motif, suggesting that Vpr and SNF2h interact through this motif.

Chromatin recruitment of Vpr depended on SNF2h

To prove that SNF2h was involved in the chromatin recruitment of Vpr, RNA-interference experiments using siRNA were carried out. When *SNF2h* siRNA was introduced into HEK293T cells, the level of protein expression of endogenous SNF2h decreased to 20% of the control level (Fig. 3a, lane 2). Under the same conditions, the amount of chromatin-bound Vpr was reduced to about 30% of control (Fig. 3a, lane 2). Together with data that the expression level of Vpr in whole cell extracts was not decreased (Fig. 3a), we conclude that SNF2h is per se involved in the chromatin loading of Vpr.

Depletion of endogenous SNF2h reduced Vpr-induced DSBs

The effects of downregulated expression of endogenous SNF2h on the biological function of Vpr were further examined. Using MIT-23 cells, in which Vpr expression was tightly regulated by the tetracycline promoter (Shimura et al. 1999a), we first checked the effects of *SNF2h* siRNA on Vpr-induced cell cycle perturbation. As shown in Fig. 3b,

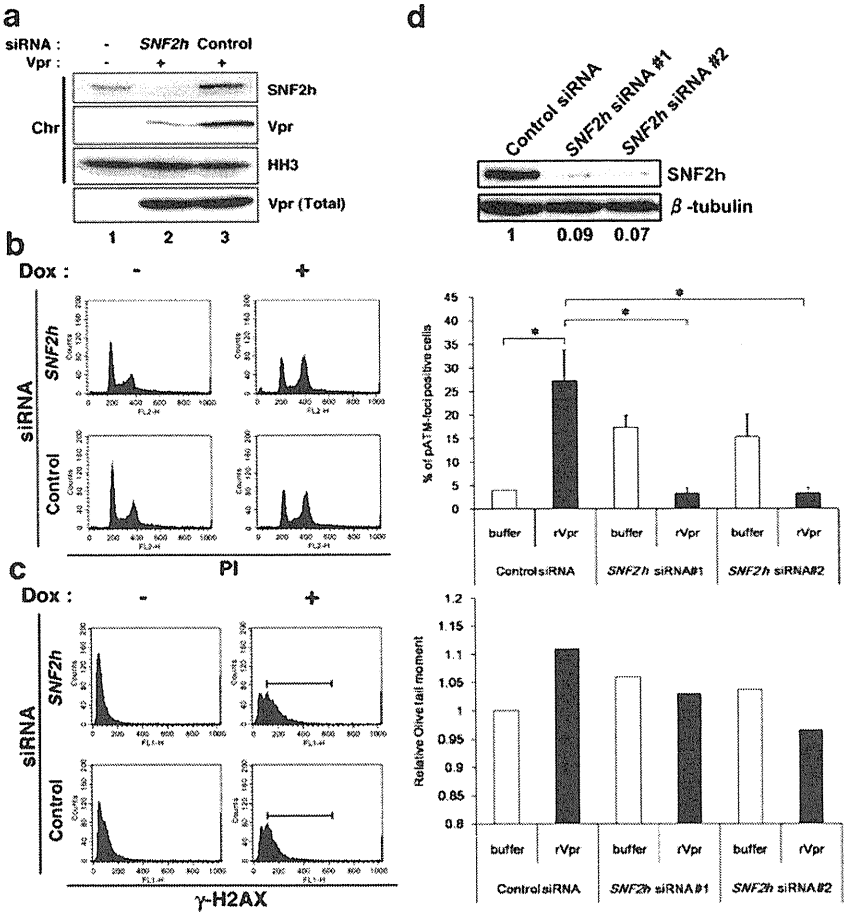

Fig. 3 SNF2h is involved in chromatin recruitment of Vpr. **a** Effects of *SNF2h* siRNA on the endogenous expression of SNF2h and chromatin recruitment of Vpr. HEK293T cells were transfected with pCMV-Vpr with control (#AM4637) or *SNF2h* siRNAs (#10620312). Chromatin fraction was prepared and subjected to WB. *Lane 1* vector control, *lane 2* pCMV-Vpr with *SNF2h* siRNA, *lane 3* pCMV-Vpr with control siRNA. **b**, **c** Effects of *SNF2h* siRNA on Vpr-induced cell cycle perturbation (**b**) and the expression of γH2AX (**c**). MIT-23 cells were cultured without or with DOX· under downregulated expression of endogenous SNF2h. Cell cycle was analyzed by PI staining, and γ-H2AX was detected by its antibody. **d** Reduction of rVpr-induced DSBs under the enhanced downregulation of endogenous SNF2h. *Top panel* WB analysis of endogenous SNF2h. TIG-3 cells were transfected twice with *SNF2h* siRNAs. On day 3 after transfection, cell extracts were subjected to analysis. As internal control, β-tubulin was detected, and the signal intensity of SNF2h was normalized by that of β-tubulin. Endogenous SNF2h was reduced to less than 10% of control by two siRNAs (s16081 and s16083). *Numbers* indicate relative level of endogenous SNF2h protein compared to the control. *Middle panel* effects of *SNF2h* siRNAs on rVpr-induced focus formation of pATM. After double transfection of *SNF2h* siRNAs, rVpr was added and numbers of pATM-foci positive cells, which had more than 8 pATM-foci/cell, were counted on the next day (Suzuki et al. 2006). Three sets of more than 50 cells were counted in each sample and subjected to statistical analysis (Student's *t*-test: one representative result of three independent experiments was shown). Mean numbers of pATM-foci positive cells±standard deviation were shown. Transfection of these siRNAs (s16081 and s16083) significantly reduced the numbers of cells positive for pATM foci (*, $P<0.05$). *Bottom panel* downregulation of endogenous SNF2h suppressed rVpr-induced DSBs judged by neutral Comet assay. Under the same conditions (*middle panel*), Comet assay was done. More than 50 cells were analyzed in each sample one representative result of two independent experiments was shown). Transfection of the siRNAs (s16081 and s16083) reduced the amount of rVpr-induced DSBs

cell cycle arrest at G_2/M phase was not attenuated by *SNF2h* siRNA. Additionally, numbers of γH2AX-positive cells were not significantly changed with or without *SNF2h* siRNA (Fig. 3c). We next examined whether Vpr-induced focus formation of pATM was affected by the siRNA. However, we did not detect apparent changes of numbers of pATM-positive cells after introduction of *SNF2h* siRNA (Suppl. Fig. 1).

To examine whether *SNF2h* siRNA were effective on the Vpr function under resting status, TIG-3 cells were serum-starved; cells entered at G_0 cell cycle phase. Then, the effect of *SNF2h* siRNA was studied. In this experiment, we examined the effects of rVpr added into the culture medium of cells. Consistent with our previous report (Nakai-Murakami et al. 2007), exogenously added rVpr induced the focus formation of pATM (Suppl.

Fig. 1, left panel, upper right panel). The increase of pATM-foci positive cells was statistically significant (Suppl. Fig. 1, right panel, $P<0.05$). We also observed that numbers of rVpr-induced pATM-foci positive cells increased by the transfection of *SNF2h* siRNA. Single transfection of *SNF2h* siRNA reduced the expression level of endogenous SNF2h to about 20% of the control level but did not inhibit rVpr-induced DSBs (Suppl. Fig. 1, right panel).

It could be possible that 20% of endogenous SNF2h was good enough for the Vpr function, and we transfected the siRNA twice and successfully reduced the protein level of endogenous SNF2h to less than 10% of the control level (Fig. 3d, top panel). In this case, rVpr-induced focus formation of pATM was decreased, which was further demonstrated by neutral Comet assay (Fig. 3d, middle and bottom panels). Based on these observations, we conclude that SNF2h is positively involved in the induction of DSBs by Vpr.

Discussion

SNF2h is a novel binding factor of Vpr and its biological relevance

Here, we newly identified SNF2h as a binding molecule of Vpr involved in the chromatin recruitment. Vpr and SNF2h were associated within cells, and in vitro experiments using recombinant proteins revealed that Vpr and SNF2h interacted directly. A Vpr mutant lacking amino acids 71–75 did not bind SNF2h, suggesting that the HFRIG motif is involved in the molecular interaction of these molecules. Consistent with the observation that SNF2h was present in the chromatin fraction, the downregulation of endogenous SNF2h by siRNA remarkably reduced the amount of Vpr in the chromatin fraction. Single transfection of *SNF2h* siRNA reduced the level of endogenous protein to about 20% of the original level, and concomitantly, chromatin-bound Vpr decreased to about 30% of the control.

Under reduced expression of endogenous SNF2h, we examined Vpr-induced DSBs. We reported that Vpr-induced DSB, and in the current work, we first confirmed that pATM-foci positive cells were induced when rVpr was exogenously added to the culture medium of TIG-3 cells (Fig. 3d). We then compared numbers of rVpr-induced pATM-foci positive cells before and after transfecting *SNF2h* siRNA. In the initial experiment, rVpr-induced foci of pATM were observed at the frequency comparable to that with control siRNA (Suppl. Fig 2, $P<0.16$). In this experiment, we treated TIG-3 cells with the siRNA by a single transfection and observed that endogenous SNF2h was downregulated to about 20% of the control level. In order to reduce the endogenous protein to the maximum extent, we transfected cells twice with the siRNA and successfully downregulated the expression level to less than 10% of control. In this case, numbers of rVpr-induced pATM-foci positive cells significantly decreased. The effect of *SNF2h* siRNA was further proved by neutral Comet assay, which is a sensitive assay system to detect DSBs (Fairbairn et al. 1995).

SNF2h is a chromatin-remodeling factor related to a variety of biological phenomena. Intriguingly, SNF2h cooperates with ACF1, a counterpart of SNF2h and is involved in the DNA replication at late S-phase in the centromeric region (Collins et al. 2002). Without SNF2h, ACF1 is not loaded to the centromere, resulting in the defects of DNA replication at the corresponding region. Data imply that the chromatin remodeling, which is directed by the complex of SNF2h and ACF1, is coordinated with DNA replication. Additionally, it has been shown that SNF2h modifies nucleosomes and generates nucleosome-free region by sliding nucleosomes (Racki and Narlikar 2008), implying that the chromatin remodeling by SNF2h is required also for Vpr-induced DSBs.

Among Vpr-associating molecules, there are several candidates that might be involved in the chromatin recruitment of Vpr (Felzien et al. 1998; Kino et al. 2002; Le Rouzic et al. 2007). Kino et al. (2002) reported that the glucocorticoid receptor, a nuclear receptor, bound Vpr and was involved in the Vpr-induced transcription from the LTR of HIV-1. Nitahara-Kasahara et al. (2007) reported that importin α (Imp-α) functions as a novel cellular factor for nuclear trafficking of Vpr. They further identified that hematoxylin, an inhibitor to the interaction of Imp-α and Vpr, attenuated the viral infection into macrophages (Suzuki et al. 2009). As an interesting observation, we recently found that Vpr induces the retrotransposition of long interspersed nucleotide element 1 (L1) in a manner depending on the aryl hydrocarbon receptor (AhR; Okudaira et al., unpublished data). Immunoprecipitation followed by Western blot analysis revealed that Vpr associates with AhR, and L1-encoded open reading frame-1 binds AhR. Data suggest that Vpr and L1 components are recruited to chromatin in a manner depending on AhR. Together, these observations indicate that Vpr utilize different cellular proteins for the chromatin recruitment, implying that the combined siRNAs targeting *SNF2h*, *AhR*, and *Imp-α* would more effectively block rVpr-induced DSBs.

Induction of DSBs is coupled with viral infection

It is important to note that lentivirus infection evokes DSB signals (Daniel et al. 2003; Lau et al. 2005). Because the discontinuity is inevitably induced during integration of proviral DNA, an eminently reasonable hypothesis is that DSB signals might be a result of viral infection (Sakurai et

al. 2009). As supportive evidence, it has been proposed that at the integration step of viral DNA into host genome, short gaps of single-stranded DNA are formed in the junction of host and viral DNAs (Skalka and Katz 2005). Repair enzymes for filling the gaps must be supplied by host cells (Daniel et al. 2004; Smith et al. 2008); otherwise, infected cells undergo apoptosis in a manner-dependent on the integrase activity of HIV-1 (Smith et al. 2008). Moreover, it has been shown that DNA-dependent protein kinase and non-homologous end joining repair pathway were required for the viral infection (Daniel et al. 1999, 2004). Consistently, it was shown that caffeine and caffeine-related methylxanthines, which are known to inhibit the ATM and ATR kinases, inhibit HIV-1 replication (Nunnari et al. 2005). Additionally, Smith et al. (2007) demonstrated that pentoxyphylline, a chemically modified methylxanthines, suppresses HIV-1 transduction without remarkable effects on the late products of the virus. Originally, pentoxyphylline-dependent inhibition of the viral replication was attributed to the blockage of TNF-α production (Peterson et al. 1992), but it was recently shown that the inhibition of viral transduction by pentoxyphylline was coupled with the inhibition of cellular ATR activity (Smith et al. 2008). As more direct evidence, Lau et al. (2005) reported that an ATM inhibitor reduced viral infection remarkably. These observations lend support to the notion that cellular responses to DSBs are critically involved in HIV-1 transduction.

We also observed that DSB-dependent cellular signals were induced during HIV-1 infection (Shimura et al. 1999b) and identified that viral infection with the lentivirus containing the wild-type Vpr induced fragmentation of the genomic DNA in the infected cells (Tachiwana et al. 2006). Moreover, the expression of Vpr as a single gene induced the focus formation of Rad51, BRCA1, pATM, and phosphorylation of Chk1/2 (Nakai-Murakami et al. 2007). Additionally, the rate of homologous recombination increased under Vpr expression. These data indicate that Vpr is a viral protein responsible for DSBs. In the current work, SNF2h was identified as a required cellular factor for Vpr-induced DSBs, supporting us to approach the biological significance of Vpr-induced DSBs.

Controversial roles of DSB-dependent cellular signals in viral infection

Although lines of evidence indicate that DSBs are coupled with HIV-1 infection and repair of damaged DNA is critical for the infection, it remained to be clarified whether DSBs contribute to the viral infection. As mentioned above, there are independent observations that support the importance of DSBs in the viral infection. In striking contrast, however, conflicting evidence suggests that DSB-induced cellular signals are dispensable for viral integration (Ariumi et al. 2005; Baekelandt et al. 2000; Dehart et al. 2005). Using mouse embryonal fibroblasts prepared from gene-knockout mice, Ariumi et al. (2005) proposed that DNA damage sensor molecules are not required for viral integration. Interestingly, however, they demonstrated that the ATM-dependent cellular signals upregulated the activity of Rev protein and increased viral infection (Ariumi and Trono 2006). It seems that different roles of DSBs in HIV-1 infection were observed depending on the experimental systems utilized, and recently, Yang et al. (2009) proposed that the effects of ATM/ATR inhibitors on HIV-1 transduction were different according to the cell lines analyzed. Given that DNA damage is induced spontaneously during DNA replication and the rate of DNA replication differs from one cell line to another, it might be important to use resting cells to correctly evaluate effects of DSB-dependent cellular signals on the viral infection (Smith and Daniel 2011). Furthermore, it was reported that caffeine inhibits the viral transduction into non-dividing cells or terminally differentiated cells (Daniel et al. 2005). Because Vpr has been shown to be involved in viral infection into resting macrophages (Vodicka et al. 1998), it would be important to analyze Vpr function in relation to the role of DSBs in resting macrophages.

Acknowledgments We are grateful to Dr. Hiroshi Sasaki (Jikei Medical School) for providing us with 2008 cells. This work was supported in parts by Grants-in-Aid for Research from the Ministry of Health, Labour and Welfare of Japan and for Research on Publicly Essential Drugs and Medical Devices from Japan Health Sciences Foundation Research.

Conflicts of interest The authors declare no conflicts of interest.

References

Andersen JL, Le Rouzic E, Planelles V (2008) HIV-1 Vpr: mechanisms of G2 arrest and apoptosis. Exp Mol Pathol. 85:2–10

Ariumi Y, Trono D (2006) Ataxia–telangiectasia-mutated (ATM) protein can enhance human immunodeficiency virus type 1 replication by stimulating Rev function. J Virol 80:2445–2452

Ariumi Y, Turelli P, Masutani M, Trono D (2005) DNA damage sensors ATM, ATR, DNA-PKcs, and PARP-1 are dispensable for human immunodeficiency virus type 1 integration. J Virol 79:2973–2978

Baekelandt V, Claeys A, Cherepanov P, De Clercq E, De Strooper B, Nuttin B, Debyser Z (2000) DNA-dependent protein kinase is not required for efficient lentivirus integration. J Virol 74:11278–11285

Collins N, Poot RA, Kukimoto I, Garcia-Jimenez C, Dellaire G, Varga-Weisz PD (2002) An ACF1–ISWI chromatin-remodeling complex is required for DNA replication through heterochromatin. Nat Genet 32:627–632

Daniel R, Katz RA, Skalka AM (1999) A role for DNA-PK in retroviral DNA integration. Science 284:644–647

Daniel R, Kao G, Taganov K, Greger JG, Favorova O, Merkel G, Yen TJ, Katz RA, Skalka AM (2003) Evidence that the retroviral

DNA integration process triggers an ATR-dependent DNA damage response. Proc Natl Acad Sci USA 100:4778–4783

Daniel R, Greger JG, Katz RA, Taganov KD, Wu X, Kappes JC, Skalka AM (2004) Evidence that stable retroviral transduction and cell survival following DNA integration depend on components of the nonhomologous end joining repair pathway. J Virol 78:8573–8581

Daniel R, Marusich E, Argyris E, Zhao RY, Skalka AM, Pomerantz RJ (2005) Caffeine inhibits human immunodeficiency virus type 1 transduction of nondividing cells. J Virol 79:2058–2065

Dehart JL, Andersen JL, Zimmerman ES, Ardon O, An DS, Blackett J, Kim B, Planelles V (2005) The ataxia telangiectasia-mutated and Rad3-related protein is dispensable for retroviral integration. J Virol 79:1389–1396

Fairbairn DW, Olive PL, O'Neill KL (1995) The comet assay: a comprehensive review. Mutat Res 339:37–59

Felzien LK, Woffendin C, Hottiger MO, Subbramanian RA, Cohen EA, Nabel GJ (1998) HIV transcriptional activation by the accessory protein, VPR, is mediated by the p300 co-activator. Proc Natl Acad Sci USA 95:5281–5286

Finzi D, Hermankova M, Pierson T, Carruth LM, Buck C, Chaisson RE, Quinn TC, Chadwick K, Margolick J, Brookmeyer R, Gallant J, Markowitz M, Ho DD, Richman DD, Siliciano RF (1997) Identification of a reservoir for HIV-1 in patients on highly active antiretroviral therapy. Science 278:1295–1300

Frulloni L, Lunardi C, Simone R, Dolcino M, Scattolini C, Falconi M, Benini L, Vantini I, Corrocher R, Puccetti A (2009) Identification of a novel antibody associated with autoimmune pancreatitis. N Engl J Med 361:2135–2142

Glotzer M, Murray AW, Kirschner MW (1991) Cyclin is degraded by the ubiquitin pathway. Nature 349:132–138

Goh WC, Rogel ME, Kinsey CM, Michael SF, Fultz PN, Nowak MA, Hahn BH, Emerman M (1998) HIV-1 Vpr increases viral expression by manipulation of the cell cycle: a mechanism for selection of Vpr in vivo. Nat Med 4:65–71

Hakimi MA, Bochar DA, Schmiesing JA, Dong Y, Barak OG, Speicher DW, Yokomori K, Shiekhattar R (2002) A chromatin remodelling complex that loads cohesin onto human chromosomes. Nature 418:994–998

He J, Choe S, Walker R, Di Marzio P, Morgan DO, Landau NR (1995) Human immunodeficiency virus type 1 viral protein R (Vpr) arrests cells in the G2 phase of the cell cycle by inhibiting p34cdc2 activity. J Virol 69:6705–6711

Heinzinger NK, Bukinsky MI, Haggerty SA, Ragland AM, Kewalramani V, Lee MA, Gendelman HE, Ratner L, Stevenson M, Emerman M (1994) The Vpr protein of human immunodeficiency virus type 1 influences nuclear localization of viral nucleic acids in nondividing host cells. Proc Natl Acad Sci USA 91:7311–7315

Hoshino S, Sun B, Konishi M, Shimura M, Segawa T, Hagiwara Y, Koyanagi Y, Iwamoto A, Mimaya J, Terunuma H, Kano S, Ishizaka Y (2007) Vpr in plasma of HIV type 1-positive patients is correlated with the HIV type 1 RNA titers. AIDS Res Hum Retroviruses 23:391–397

Hoshino S, Konishi M, Mori M, Shimura M, Nishitani C, Kuroki Y, Koyanagi Y, Kano S, Itabe H, Ishizaka Y (2010) HIV-1 Vpr induces TLR4/MyD88-mediated IL-6 production and reactivates viral production from latency. J Leukoc Biol 87:1133–1143

Izuta H, Ikeno M, Suzuki N, Tomonaga T, Nozaki N, Obuse C, Kisu Y, Goshima N, Nomura F, Nomura N, Yoda K (2006) Comprehensive analysis of the ICEN (interphase centromere complex) components enriched in the CENP-A chromatin of human cells. Genes Cells 11:673–684

Kino T, Gragerov A, Slobodskaya O, Tsopanomichalou M, Chrousos GP, Pavlakis GN (2002) Human immunodeficiency virus type 1 (HIV-1) accessory protein Vpr induces transcription of the HIV-1 and glucocorticoid-responsive promoters by binding directly to p300/CBP coactivators. J Virol 76:9724–9734

Lai M, Zimmerman ES, Planelles V, Chen J (2005) Activation of the ATR pathway by human immunodeficiency virus type 1 Vpr involves its direct binding to chromatin in vivo. J Virol 79:15443–15451

Lau A, Swinbank KM, Ahmed PS, Taylor DL, Jackson SP, Smith GC, O'Connor MJ (2005) Suppression of HIV-1 infection by a small molecule inhibitor of the ATM kinase. Nat Cell Biol 7:493–500

Le Rouzic E, Belaidouni N, Estrabaud E, Morel M, Rain JC, Transy C, Margottin-Goguet F (2007) HIV1 Vpr arrests the cell cycle by recruiting DCAF1/VprBP, a receptor of the Cul4-DDB1 ubiquitin ligase. Cell Cycle 6:182–188

Lusser A, Kadonaga JT (2003) Chromatin remodeling by ATP-dependent molecular machines. Bioessays 25:1192–1200

Nakai-Murakami C, Shimura M, Kinomoto M, Takizawa Y, Tokunaga K, Taguchi T, Hoshino S, Miyagawa K, Sata T, Kurumizaka H, Yuo A, Ishizaka Y (2007) HIV-1 Vpr induces ATM-dependent cellular signal with enhanced homologous recombination. Oncogene 26:477–486

Nakai-Murakami C, Minemoto Y, Ishizaka Y (2009) Vpr-induced DNA double-strand breaks: molecular mechanism and biological relevance. Curr HIV Res 7:109–113

Nitahara-Kasahara Y, Kamata M, Yamamoto T, Zhang X, Miyamoto Y, Muneta K, Iijima S, Yoneda Y, Tsunetsugu-Yokota Y, Aida Y (2007) Novel nuclear import of Vpr promoted by importin alpha is crucial for human immunodeficiency virus type 1 replication in macrophages. J Virol 81:5284–5293

Niwa H, Abe K, Kunisada T, Yamamura K (1996) Cell-cycle-dependent expression of the STK-1 gene encoding a novel murine putative protein kinase. Gene 169:197–201

Nunnari G, Argyris E, Fang J, Mehlman KE, Pomerantz RJ, Daniel R (2005) Inhibition of HIV-1 replication by caffeine and caffeine-related methylxanthines. Virology 335:177–184

Peterson PK, Gekker G, Chao CC, Schut R, Verhoef J, Edelman CK, Erice A, Balfour HH Jr (1992) Cocaine amplifies HIV-1 replication in cytomegalovirus-stimulated peripheral blood mononuclear cell cocultures. J Immunol 149:676–680

Poot RA, Bozhenok L, van den Berg DL, Steffensen S, Ferreira F, Grimaldi M, Gilbert N, Ferreira J, Varga-Weisz PD (2004) The Williams syndrome transcription factor interacts with PCNA to target chromatin remodelling by ISWI to replication foci. Nat Cell Biol 6:1236–1244

Porcedda P, Turinetto V, Brusco A, Cavalieri S, Lantelme E, Orlando L, Ricardi U, Amoroso A, Gregori D, Giachino C (2008) A rapid flow cytometry test based on histone H2AX phosphorylation for the sensitive and specific diagnosis of ataxia telangiectasia. Cytom A 73:508–516

Racki LR, Narlikar GJ (2008) ATP-dependent chromatin remodeling enzymes: two heads are not better, just different. Curr Opin Genet Dev 18:137–144

Sakurai Y, Komatsu K, Agematsu K, Matsuoka M (2009) DNA double strand break repair enzymes function at multiple steps in retroviral infection. Retrovirology 6:114

Shimura M, Tanaka Y, Nakamura S, Minemoto Y, Yamashita K, Hatake K, Takaku F, Ishizaka Y (1999a) Micronuclei formation and aneuploidy induced by Vpr, an accessory gene of human immunodeficiency virus type 1. FASEB J 13:621–637

Shimura M, Onozuka Y, Yamaguchi T, Hatake K, Takaku F, Ishizaka Y (1999b) Micronuclei formation with chromosome breaks and gene amplification caused by Vpr, an accessory gene of human immunodeficiency virus. Cancer Res 59:2259–2264

Skalka AM, Katz RA (2005) Retroviral DNA integration and the DNA damage response. Cell Death Differ 12(Suppl 1):971–997

Smith JA, Daniel R (2011) Up-regulation of HIV-1 transduction in nondividing cells by double-strand DNA break-inducing agents. Biotechnol Lett 33:243–252

Smith JA, Nunnari G, Preuss M, Pomerantz RJ, Daniel R (2007) Pentoxifylline suppresses transduction by HIV-1-based vectors. Intervirology 50:377–386

Smith JA, Wang FX, Zhang H, Wu KJ, Williams KJ, Daniel R (2008) Evidence that the Nijmegen breakage syndrome protein, an early sensor of double-strand DNA breaks (DSB), is involved in HIV-1 post-integration repair by recruiting the ataxia telangiectasia-mutated kinase in a process similar to, but distinct from, cellular DSB repair. Virol J 5:11

Suzuki K, Okada H, Yamauchi M, Oka Y, Kodama S, Watanabe M (2006) Qualitative and quantitative analysis of phosphorylated ATM foci induced by low-dose ionizing radiation. Radiat Res 165:499–504

Suzuki T, Yamamoto N, Nonaka M, Hashimoto Y, Matsuda G, Takeshima SN, Matsuyama M, Igarashi T, Miura T, Tanaka R, Kato S, Aida Y (2009) Inhibition of human immunodeficiency virus type 1 (HIV-1) nuclear import via Vpr–Importin alpha interactions as a novel HIV-1 therapy. Biochem Biophys Res Commun 380:838–843

Tachiwana H, Shimura M, Nakai-Murakami C, Tokunaga K, Takizawa Y, Sata T, Kurumizaka H, Ishizaka Y (2006) HIV-1 Vpr induces DNA double-strand breaks. Cancer Res 66:627–631

van Zon W, Ogink J, ter Riet B, Medema RH, te Riele H, Wolthuis RM (2010) The APC/C recruits cyclin B1-Cdk1-Cks in prometaphase before D box recognition to control mitotic exit. J Cell Biol 190:587–602

Vodicka MA, Koepp DM, Silver PA, Emerman M (1998) HIV-1 Vpr interacts with the nuclear transport pathway to promote macrophage infection. Genes Dev 12:175–185

Wong JK, Hezareh M, Gunthard HF, Havlir DV, Ignacio CC, Spina CA, Richman DD (1997) Recovery of replication-competent HIV despite prolonged suppression of plasma viremia. Science 278:1291–1295

Yang YX, Guen V, Richard J, Cohen EA, Berthoux L (2009) Cell context-dependent involvement of ATR in early stages of retroviral replication. Virology 396:272–279

JOURNAL OF VIROLOGY, Jan. 2011, p. 932–945
0022-538X/11/$12.00 doi:10.1128/JVI.01668-10

Vol. 85, No. 2

Identification of Amino Acids in the Human Tetherin Transmembrane Domain Responsible for HIV-1 Vpu Interaction and Susceptibility▽†

Tomoko Kobayashi,[1] Hirotaka Ode,[2] Takeshi Yoshida,[1,3] Kei Sato,[1] Peter Gee,[1] Seiji P. Yamamoto,[1,4] Hirotaka Ebina,[1] Klaus Strebel,[3] Hironori Sato,[2] and Yoshio Koyanagi[1]*

Laboratory of Viral Pathogenesis, Institute for Virus Research, Kyoto University, 53 Shogoin-kawara-cho, Sakyo-ku, Kyoto 606-8507, Japan[1]; Pathogen Genomics Center, National Institute of Infectious Diseases, 4-7-1 Gakuen, Musashimurayama, Tokyo 208-0011, Japan[2]; Laboratory of Molecular Microbiology, Viral Biochemistry Section, National Institute of Allergy and Infectious Diseases, NIH, Bethesda, Maryland 20892-0460[3]; and Department of Molecular and Cellular Biology, Graduate School of Biostudies, Kyoto University, Japan 53 Shogoin-kawara-cho, Sakyo-ku, Kyoto 606-8507, Japan[4]

Received 9 August 2010/Accepted 28 October 2010

Tetherin, also known as BST-2/CD317/HM1.24, is an antiviral cellular protein that inhibits the release of HIV-1 particles from infected cells. HIV-1 viral protein U (Vpu) is a specific antagonist of human tetherin that might contribute to the high virulence of HIV-1. In this study, we show that three amino acid residues (I34, L37, and L41) in the transmembrane (TM) domain of human tetherin are critical for the interaction with Vpu by using a live cell-based assay. We also found that the conservation of an additional amino acid at position 45 and two residues downstream of position 22, which are absent from monkey tetherins, are required for the antagonism by Vpu. Moreover, computer-assisted structural modeling and mutagenesis studies suggest that an alignment of these four amino acid residues (I34, L37, L41, and T45) on the same helical face in the TM domain is crucial for the Vpu-mediated antagonism of human tetherin. These results contribute to the molecular understanding of human tetherin-specific antagonism by HIV-1 Vpu.

Intrinsic immune molecules have been discovered in mammalian cells that restrict retrovirus replication (64). Tetherin, also known as BST-2/CD317/HM1.24, is a host factor that recently has been identified as a potent inhibitor against the release of HIV-1 particles (46, 67). The retained particles then are internalized into the endosomes/lysosomes and presumably degraded (4). HIV-1 is able to elude the tetherin-driven defense mechanism by expressing viral protein U (Vpu), which is expressed in a unique lineage of primate lentiviruses (64). Vpu is an 81-amino-acid (aa) type 1 integral membrane protein encoded together with the *env* gene from a bicistronic mRNA, and it promotes the release of HIV-1 particles by specifically antagonizing tetherin (7, 63, 65). It has been shown that Vpu inhibits the cell surface expression of tetherin by its relocalization to the *trans*-Golgi network (TGN) and the recycling endosomes (12), and/or by targeting it for the proteosomal and/or lysosomal degradation in a beta-transducin repeat-containing protein (β-TrCP)-dependent manner (10, 41). β-TrCP is a component of an E3 ubiquitin ligase complex that also is involved in the Vpu-induced proteasomal degradation of CD4 via the endoplasmic reticulum (ER)-associated degradation (ERAD) pathway (64, 65, 70). An amino acid alignment of representative primate lentiviral Vpus shows that they are highly variable and have functional differences (38, 57). Only Vpu from HIV-1 pandemic group M and nonpandemic group N strains, but not from HIV-1 group O and SIVcpz, can counteract human tetherin (hu-tetherin) activity (57). These studies suggested that the evolution of a fully functional anti-tetherin protein, such as the highly adapted Vpu of the group M strains, is an important prerequisite for the ongoing spread of HIV-1 in the human population. The anti-tetherin function of HIV-1 group M Vpu is highly specific to tetherin from human, chimpanzee, and gorilla (57). Vpu does not counteract tetherin homologues from different species such as mouse, rhesus macaques, and African green monkey (agm) (17, 43). Until now, research on the interplay between hu-tetherin and Vpu has been limited mainly to the amino acid residues within the TM that appear to be important for the interaction and susceptibility of tetherin to Vpu (10, 18, 43, 54). However, whether these reported amino acid residues also play a role in the Vpu association, and whether there are other determinants of the interaction, remain to be elucidated. Thus, we set out to understand the parameters of the hu-tetherin-Vpu interaction.

Using bimolecular fluorescence complementation (BiFC) (31) and site-directed mutagenesis, we first identified three amino acid residues (I34, L37, and L41) within the TM region of human tetherin (hu-tetherin) that are crucial for its interaction with Vpu in live cells. The alteration of any one of these amino acid residues leads to a significantly reduced interaction with Vpu and also a loss of Vpu response in the virus release assay. Furthermore, structural and functional roles of these amino acid were addressed with molecular dynamics (MD) simulations of the TM domain of hu- and agm-tetherins in a lipid bilayer environment. To our knowledge, this is the first report showing the amino acid residues in hu-tetherin essential

* Corresponding author. Mailing address: Laboratory of Viral Pathogenesis, Institute for Virus Research, Kyoto University, 53 Shogoin-kawahara-cho, Sakyo-ku, Kyoto 606-8507, Japan. Phone: 81-75-751-4811. Fax: 81-75-751-4812. E-mail: ykoyanag@virus.kyoto-u.ac.jp.

† Supplemental material for this article may be found at http://jvi.asm.org/.

▽ Published ahead of print on 10 November 2010.

for interaction with Vpu in live cells, and we found that the proper positioning of these residues is regulated by the presence of two upstream amino acid residues in the TM helix.

MATERIALS AND METHODS

Plasmids. The human, mouse, and agm *tetherin* cDNA was amplified by reverse transcription-PCR (RT-PCR) from human peripheral blood lymphocyte (PBL), NIH 3T3, or COS-7 cells, respectively, and subcloned into Kusabira green (KG) fragment-encoding plasmids phmKGC-MC and phmKGN-MC (MBL). From pcDNA-Vphu, expressing a codon-optimized and Rev-independent HIV-1_{NL4-3} Vpu protein (47), an *orf* fragment of Vphu also was inserted into phmKGN-MN. A KGN-hu-tetherin fragment and KGN-Vphu were subcloned into CSII-CDF-GATEWAY-IRES-H2Kk (30). The mutated hu-, mo-, and agm-tetherin DNA were created by overlap extension PCR. All constructs were confirmed by DNA sequencing. A list of fusion proteins of tetherin and Vpu is summarized in Fig. 1A.

Cell culture, transfection, and transduction. HEK 293 cells or its derivatives were cultured in Dulbecco's modified Eagle's medium (DMEM) supplemented with 10% fetal bovine serum and antibiotics. Cells were transfected by calcium phosphate DNA precipitation or Lipofectamine 2000 reagent (Invitrogen) according to the manufacturer's protocol. Stably KGN-Vpu or KGC-hu-tetherin-expressing HEK 293 was generated by a lentiviral vector as described before (30). The amount of plasmid DNA for transfection was normalized to 1.4 μg per well by pcDNA3.1. Recombinant human alpha interferon (IFN-α) was purchased from Prospec.

Confocal microscopy. HEK 293 cells were transfected by an individual or selected pairs of BiFC constructs (0.5 μg of each plasmid). At 24 h posttransfection, cells were stained with Hoechst 33342 (Invitrogen) and fixed with 2% paraformaldehyde, followed by treatment with 0.05% saponin. Cells were sequentially incubated with monoclonal antibodies (MAbs) against GM130, p230, EEA1, Rab4, CD63, or LAMP1 (BD Transduction), followed by incubation with a goat anti-mouse IgG MAb (Molecular probes). The recycling endosomes were visualized as previously reported (12). Cells were analyzed as described before (71). All of the images were taken under similar experimental conditions (i.e., exposure time, magnification, and intensification), and image processing was the same for all of the images shown in the figure.

Immunoblot analysis. At 24 h posttransfection, cells were lysed and the lysates were processed as described before (56). The membrane was incubated with anti-KGN, anti KGC MAb (MBL), anti-Flag MAb (Sigma), anti-Vpu, or anti-p24 antibody (40, 56), and then horseradish peroxidase-conjugated goat anti-mouse immunoglobulin G (Santa Cruz Biotechnology). The immune complex was visualized using an enhanced chemiluminescence system (LAS 4000) according to the instructions provided by the manufacturer.

Flow cytometry. HEK 293 cells were transfected either individually or in selected pairs of BiFC construct (0.5 μg of each plasmid) 24 h posttransfection, harvested, and analyzed as described previously (71).

Tetherin activity and Vpu sensitivity assays. HEK 293 cells were transfected using Lipofectamine 2000 (Invitrogen) with 1 μg of pNL4-3 (wild type [WT]) or pNL4-3/Udel (Vpu deletion mutant) HIV-1 infectious plasmids (34), KGC-tagged tetherin, and its derivative plasmids. Cells and supernatants were harvested 24 h after transfection. The supernatants were filtered and infectious virion yields were measured using TZM-bl indicator cells, as described before (56), and given in relative light units (RLU).

Statistical analysis. The Mann-Whitney's U test and Student's *t* test were used to determine statistical significance.

Construction of initial model for MD simulation of helix model of the tetherin TM domain in a lipid bilayer environment. To perform MD simulations (29), we first prepared seven initial models roughly mimicking helical structures of the tetherin TM domains (hu-tetherin, agm-tetherin, agm-LL, agm-LL/I45T, hu-T45I, hu-delGI, and hu-delGI/T45I) under a lipid bilayer environment (28, 61). First, we constructed a helix peptide (D15 to C53 in hu-tetherin) in the range from the six amino acids upstream of the TM domain (K21 to K47 in hu-tetherin) to its six amino acids downstream in each tetherin, using the LEaP module of AMBER9 (35, 51). In addition, acetyl- and *N*-methyl groups were connected to the N- and C-terminal ends of the peptide, respectively. We also prepared a bilayer membrane structure, including about 120 palmitoyl-oleyl-*sn*-phosphatidyl-cholines (POPC), using VMD 1.8.7 (22). POPC is the largest component in the cellular membrane of the mammalian cell (5, 68). Finally, the helical peptide was perpendicularly inserted into the membrane, and about 10,000 water molecules were placed on both sides of the membrane surface using the LEaP module. In this study, we applied the TIP3P water model (27) as the water molecule. The AMBER ff99SB force field (20) was applied to energy and force calculations for peptide and water molecules, and the gaff (69) was used for POPC (26). The atom types and charges of each atom in POPC were automatically assigned using the Antechamber module of AMBER9 (35, 51).

MD simulations of the tetherin TM domain in a lipid bilayer environment. Prior to MD simulations of each of seven helix models, we performed the energy minimization of the initial model and heated it until 36.85°C (310 K). The energy minimization was achieved by 1,000 steps of the steepest-descent method and by the subsequent 1,000 steps of the conjugated gradient method to release steric clashes. The minimized model subsequently was heated using Langevin dynamics (39, 50) with a collision frequency of 5.0 ps^{-1} (10^{-12} s) with the NVT ensemble for 0.1 ns (10^{-9} s). Preliminary MD simulation then was performed at 36.85°C under 1 atm pressure with the NPT ensemble for 0.5 s. Temperature was controlled using Langevin dynamics (39, 50) with a collision frequency of 1.0 ps^{-1}. Until this step, to achieve equilibration for the membrane prior to that for peptide, the helical structure of the peptide was constrained. The distance of the hydrogen bond pair between main chains of the helical peptide was forced to be less than 3.0 Å with a weak constraint by a harmonic potential of 2.5 kcal/mol/Å^2. We further performed 4.5 ns of MD simulations without constraints of hydrogen bonds in the peptides.

Throughout the simulations, we also applied the following conditions. In the models there are many highly charged atoms, like phosphate groups in lipids. The highly charged nature of phosphate groups tends to prevent simulations from leading to stable structures having a nanosecond lifetime (16, 23, 44, 48). To avoid the unexpected effects, the additional weak forces were applied between hetero-atoms (N, O, and S atoms) in the peptide side chain of extracellular loop (ECL) (D15 to K21 or K47 to E53 in hu-tetherin) and phosphorus atoms in lipids to weaken the electrostatic interactions of highly charged phosphate atoms, using a harmonic potential of 2.5 kcal/mol/Å^2 with an equilibration distance of 7.0 Å when the distance between them was less than 7.0 Å. In addition, the periodic boundary condition was applied to avoid edge effects on the boundary face. The particle mesh Ewald (PME) method (8, 9, 15) is used for calculating the electrostatic energy of a periodic box. The cutoff distance of the nonbonded energy term was set to 12.0 Å. The movement of bonds involving hydrogen atoms was constrained by the SHAKE algorithm (55). The time step was set to 2.0 fs (10^{-15} s). The simulations were achieved with the PMEMD module of AMBER9 (35, 51).

Lastly, we evaluated the equilibration of the model. After 2.0 ns of MD simulation, each membrane thickness and root mean squared distance (RMSD) from a heated structure got close to a certain value (see Fig. S3 in the supplemental material). Furthermore, to validate the equilibration of peptide conformation at the C-terminal half of the TM domain (G27 to E51 in hu-tetherin), 3,000 snapshots were derived from 2.0 to 5.0 ns of MD simulation and were grouped into five clusters by the Bayesian algorithm (60) using the AMBER tool 1.2 in each model. Since the representative structure in the largest cluster is similar to the representative structures in the other four clusters (RMSD < 2.0 Å), we considered that conformations of the C-terminal domain were well equilibrated (see Table S1 in the supplemental material). In this study, among the 3,000 snapshots in each model, we selected a representative structure using the Bayesian clustering algorithm (60) to analyze its structural feature.

Comparison of 3D models of the tetherin TM domains. We compared three-dimensional (3D) structures of the hu-tetherin TM models to those of other TM variants by following the procedure of PyMOL version 0.99 rc6 (http://www.pymol.org/) (Schrödinger LLC). We first fitted models to the hu-tetherin model using the coordinates of main-chain atoms (N, Cα, and C) around C-terminal TM domains (G27 to E51 in hu-tetherin), because agm-tetherin, hu-delGI, and hu-delGI/T45I have two amino acid deletions in the N-terminal TM domains. The RMSD values for individual amino acid residues were calculated using the coordinates of the main-chain atoms in the fitted models.

RESULTS

Visualization of tetherin-Vpu heterodimer complexes in live cells. To detect tetherin-Vpu complexes in live cells, we used the BiFC technique (32) by the ectopic expression of two fragmented monomeric KG fluorescent proteins. This technique is based on the formation of a fluorescent complex from N- and C-terminal nonfluorescent fragments, KGN and KGC, which are brought together by association through interacting partner proteins fused to the fragments, thus allowing the

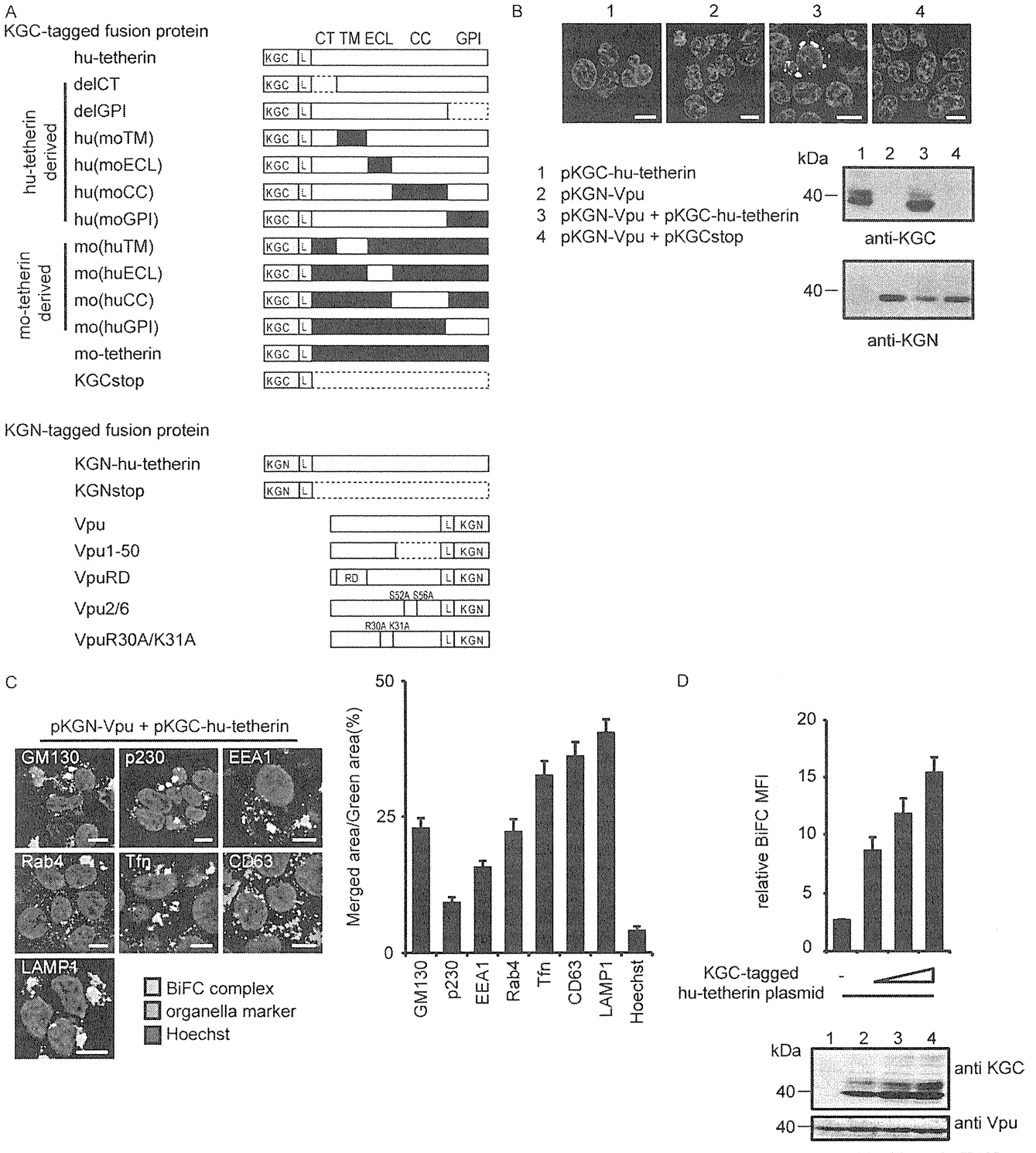

FIG. 1. Interaction of tetherin and Vpu via TM domain. (A) Schematic diagram of KGN or KGC fusion protein used in this study. KGN- or KGC-peptide tag was fused in frame to the N terminus of hu-tetherin, mo-tetherin, or mutant proteins. KGN-tag was fused in frame to the C terminus of Vpu or its mutant proteins. The L indicates a linker sequence inserted between KG fragments and proteins of interest. Human, white; mouse, black; the broken line indicates deletion residues. (B) Tetherin-Vpu complex detected by BiFC. HEK 293 cells were transfected with the indicated DNA and examined by confocal microscopy (upper) and immunoblot analysis (lower). (C) BiFC-expressing cells were stained with markers specific for each organelle and imaged by confocal microscopy. Bar, 10 μm. The ratios of the merged area between BiFC (green) and organelles (red) were quantified (right columns) for more than 100 cells. (D) Quantitative BiFC assay. The KGN-Vpu-expressing cells were transfected with pKGC-hu-tetherin (0, 100, 200, or 400 ng) or a control [pKGCstop, 400 ng] and analyzed by flow cytometry (upper) and immunoblot analysis (lower). Relative MFI values are defined as the MFI of tetherin plasmid-transfected cells minus the MFI of untransfected cells, and results represent the means from three independent experiments plus standard deviations.

TABLE 1. Surface expression of tetherin and its derivatives used in this study[a]

Name of N-terminally KGC-tagged fusion protein	MFI of tetherin
Untagged hu-tetherin	107.6 ± 12.7
hu-tetherin	117.6 ± 16.2
KGCstop	13.1 ± 6.8
mo-tetherin	ND
mo(huTM)	ND
mo(huECL)	ND
mo(huCC)	123.3 ± 6.3
mo(huGPI)	ND
hu(muTM)	115.3 ± 4.7
hu(muECL)	138.4 ± 15.0
hu(muCC)	ND
hu(muGPI)	127.9 ± 9.8
LLL(22-24)AAA	116.3 ± 14.6
GIG(25-27)AAA	138.6 ± 27.2
ILV(28-30)AAA	159.4 ± 17.7
LLI(31-33AAA	160.2 ± 19.0
IVI(34-36)AAA	142.1 ± 17.9
LGV(37-39)AAA	161.0 ± 14.1
PLI(40-42)AAA	113.9 ± 12.3
IFT(43-45)AAA	149.8 ± 8.5
IKA(46-48)AAA	117.9 ± 2.0
I34A	155.9 ± 5.9
V35A	135.1 ± 34.5
I36A	157.1 ± 18.8
L37A	141.6 ± 26.8
G38A	169.1 ± 23.6
V39A	164.5 ± 14.5
P40A	165.9 ± 4.1
L41A	140.1 ± 9.8
I42A	143.6 ± 29.1

[a] Values indicate the means from three independent experiments plus standard deviations. ND, not detected

specific visualization of interactive complexes in live cells (66). Preceding reports have indicated that a peptide tagged to the N terminus of human tetherin (hu-tetherin) or the C terminus of Vpu does not interfere with their function and localization. Therefore, we constructed the plasmid encoding KGC fused to the N-terminal end of hu-tetherin (KGC-hu-tetherin), designated pKGC-hu-tetherin. The plasmid encoding KGN was fused to the C-terminal end of codon optimized-Vpu (KGN-Vpu), designated pKGN-Vpu. The level of HIV-1 release inhibition by pKGC-hu-tetherin (data not shown) and its cell surface expression levels (Table 1) were equivalent to that of untagged hu-tetherin. In addition, pKGN-Vpu and untagged Vpu-expressing plasmid displayed similar levels of anti-tetherin activity (data not shown). We detected specific and significant fluorescence in cells coexpressing KGC-hu-tetherin and KGN-Vpu but not in those expressing either KGC-hu-tetherin or KGN-Vpu alone or KGN-Vpu and KGCstop (Fig. 1B). Immunoblot analysis confirmed the expression and proper size of the individual proteins (KGC-hu-tetherin and KGN-Vpu) (Fig. 1A and B). KGCstop and KGNstop, which are mutants with a termination codon inserted at a site upstream of the tetherin open reading frame (ORF), were used as negative controls. In the fluorescence-positive cells, little signal was seen at the plasma membrane, perhaps due to the downregulation of tetherin expression from the cell surface. By staining with antibodies or reagents specific for individual organelles within the cell, we detected BiFC signals from tetherin-Vpu complexes within organelles in which tetherin localization has been reported previously (42); however, distribution frequencies were different (Fig. 1C and data not shown). In fact, the previous study showed that little hu-tetherin was seen in vesicular compartments positive for the late endosome marker (LAMP-2), while in our study the complexes appear to localize predominantly in $CD63^+$ and $LAMP\text{-}1^+$ late endosomes (Fig. 1C, right columns) (42). These results indicate that the BiFC assay is a useful and sensitive approach to determine Vpu-tetherin interactions.

Quantitative BiFC assay for tetherin and Vpu interaction. To quantitatively measure tetherin-Vpu heterodimer complexes, we generated a HEK 293 cell line stably expressing KGN-Vpu (Fig. 1D, bottom). The mean fluorescence intensity (MFI) of the reconstituted KG fluorophore, measured by flow cytometry, is directly proportional to the number of interactive complexes in the cells (32). To examine the sensitivity of the assay with respect to hu-tetherin and Vpu complexes, the KGN-Vpu cells were transfected with various amounts of KGC-hu-tetherin plasmid DNA (Fig. 1D). The intensity of the KG BiFC signal corresponded well with the level of KGC-tetherin expression detected by an anti-KGC antibody 24 h after transfection (Fig. 1D, lanes 2 to 4, compare to the corresponding upper columns). These results demonstrate that our tetherin-Vpu BiFC assay provides sufficient sensitivity for measuring hu-tetherin-Vpu complexes.

Interaction of the TM region of hu-tetherin with Vpu. Tetherin has a unique topology: the amino-terminal cytoplasmic tail (CT) is followed by a single TM region, extracellular loop (ECL), coiled-coil domain (CC), and glycosyl phosphatidylinositol membrane anchor (GPI) at the C terminus (36). To map the domain of hu-tetherin that mediates interaction with Vpu, we first prepared KGC-tagged tetherin mutants deleted in the CT or GPI anchor (delCT and delGPI) (Fig. 1A), transfected them into the KGN-Vpu-expressing cells, and examined the resulting BiFC signals. We found that delCT and delGPI mutants produced slightly enhanced BiFC signals compared to those of WT tetherin (Fig. 2A), perhaps due to an increase in the expression level in cells (Fig. 2A, bottom) or a change in the protein localization. These data reveal that the CT and GPI regions in tetherin are not required for Vpu interaction. To investigate specific characteristics of the hu-tetherin-Vpu complex under similar topological conditions, we next used KGC-tagged mouse tetherin (KGC-mo-tetherin) (Fig. 1A). Since mo-tetherin displays resistance to Vpu counteraction (17), less interaction between Vpu and mo-tetherin was expected. In fact, the coexpression of KGN-Vpu and KGC-mo-tetherin gave no detectable fluorophore (Fig. 2B and C, lane 10), while the coexpression of KGN-tagged mo-tetherin and KGC-mo-tetherin yielded a signal (data not shown), indicating mo-tetherin homodimer formation can produce a strong fluorophore. To further verify BiFC signals, we examined the subcellular localization of Vpu and tetherin together with BiFC signals. The results showed that hu-tetherin colocalized with Vpu as well as BiFC signals (Fig. 2B, lower), whereas mo-tetherin colocalized with Vpu but did not produce BiFC florescence (Fig. 2B, upper). This indicated that BiFC signals are the results of specific interactions. These data suggest that specific region(s) of hu-tetherin participate in the interaction with Vpu. Thus, we next prepared a KGC-tagged hu- or mo-

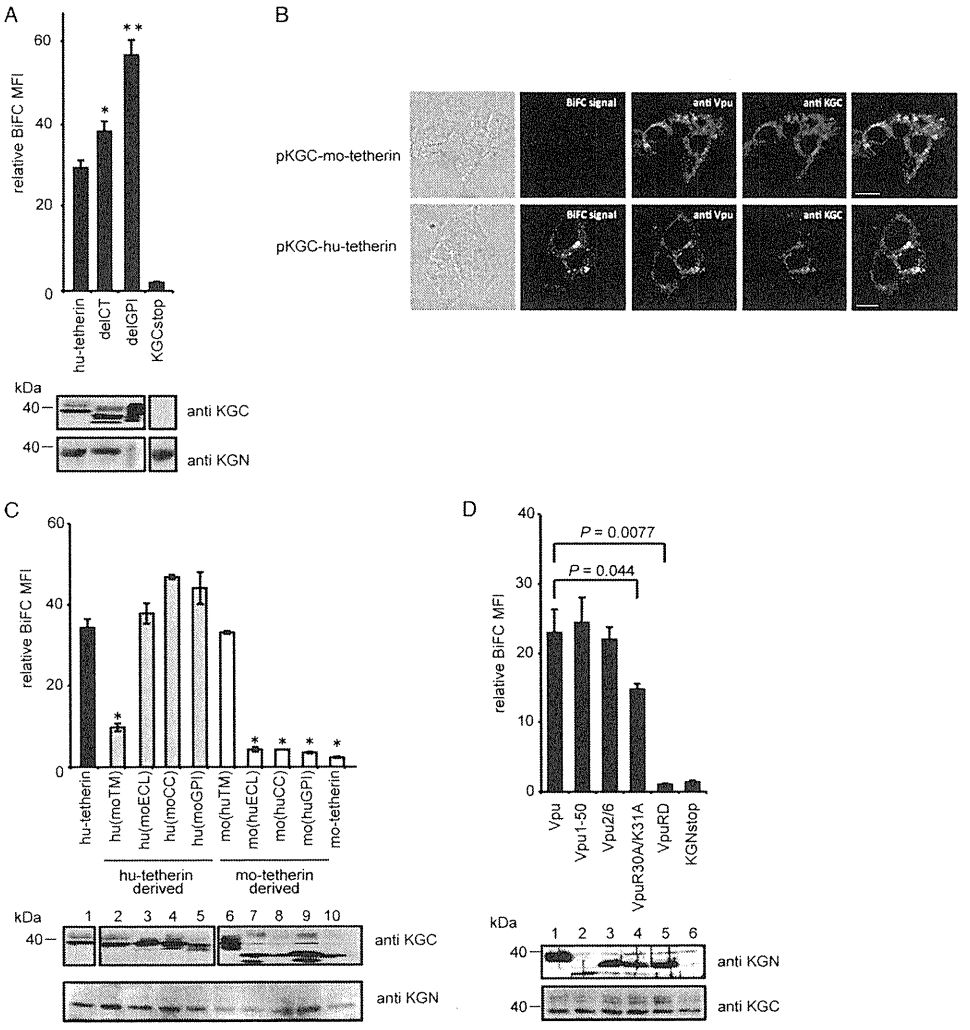

FIG. 2. Interaction of tetherin and Vpu via TM domains. (A) The KGN-Vpu-expressing cells were transfected with plasmid encoding KGC-tagged hu-tetherin or deletion mutants of CT or GPI (delCT and delGPI). The expression of KGC-tetherin fusion protein was detected using an anti-KGC antibody (bottom). Relative MFI is defined as the MFI of pKGC-tetherin-transfected or its mutant-transfected cells minus the MFI of untransfected cells, and results represent the means from three independent experiments plus standard deviations. The amount of protein applied for the delGPI Western blotting was 10 times less than that for WT hu-tetherin to avoid the overexposure of the protein on polyvinylidene difluoride membrane. Statistical significance (Student's *t* test) in the MFI of human tetherin and mutants are represented as follows: **, $P < 0.01$; *, $P < 0.05$. (B) The KGN-Vpu-expressing HEK 293 cells were transfected with pKGC-mo-tetherin (upper) or pKGC-hu-tetherin (lower). Cells were double stained with anti-Vpu antibody and anti-KGC antibody and imaged by confocal microscopy. (C) Interaction of tetherin TM with Vpu. The KGN-Vpu-expressing cells were transfected with KGC-hu-tetherin, KGC-mo-tetherin, or chimera mutant DNA containing reciprocal exchanges of the TM, ECL, CC, or GPI between the hu- and mo-tetherin proteins and analyzed by flow cytometry. Statistical significance (Student's *t* test) in the MFI of hu-tetherin and chimeras are represented as follows: *, $P < 0.01$; standard deviation for mo(huCC) was 0.0061. Relative MFI is defined as the MFI of pKGC-tetherin-transfected or its mutant-transfected cells minus the MFI of untransfected cells. (D) Interaction of the Vpu TM with tetherin. KGC-tetherin-expressing cells were transfected with KGN-Vpu or its mutant DNA and analyzed. Statistical significances (Student's *t* test) in the BiFC signals are given. Relative MFI values are defined as the MFI of pKGN-Vpu or its mutant-transfected cells minus the MFI of untransfected cells. The results represent the means from three independent experiments (A, C, and D). Expression of the KGC or KGN fusion or Vpu protein was detected by immunoblot analysis with individual antibodies (A, C, and D).

tetherin-based chimera with alterations of the TM, ECL, CC, and GPI from mo-tetherin or hu-tetherin (Fig. 1A). The subcellular localization and cell surface expression of the chimeric tetherins were detected by anti-KGC antibody or quantified using an anti-hu-tetherin antibody that reacts with the ECL domain. The anti-hu-tetherin antibody does not react with the mouse ECL domain; thus, we were only able to quantify the cell surface expression of chimera carrying the human ECL domain. The cell surface expression and localization of these chimera were similar to those of WT hu-tetherin (Table 1 and data not shown). Furthermore, we examined the total expression of the mutants by immunoblot analysis using an anti-KGC antibody. The expression of all chimeras was comparable (Fig. 2C). The mo-tetherin-based chimeric proteins migrate as multiple bands on immunoblot analysis, probably due to their differential N glycosylation (1, 17). Hu-tetherin-based chimeras with ECL, CC, or GPI domains of mo-tetherin but carrying a TM domain of hu-tetherin displayed BiFC signals compara-

ble to that of WT hu-tetherin (Fig. 2C). In contrast, the hu-tetherin-based chimera with the reciprocal TM of mo-tetherin showed a significant reduction in BiFC signal (Fig. 2C). Conversely, the mo-tetherin-based chimera with the reciprocal TM of hu-tetherin displayed significant BiFC signals similar to those of parental hu-tetherin (Fig. 2C), indicating that the TM of hu-tetherin is necessary and sufficient for the interaction between mo-tetherin-based mutants and Vpu. Mo-tetherin-based chimera mutants replaced with the ECL, CC, or GPI of hu-tetherin showed a weak signal (Fig. 2C), suggesting that the other regions are less important in the Vpu interaction.

Specific interaction of Vpu TM with hu-tetherin. HIV-1 Vpu protein consists of two major elements: an N-terminal TM domain that anchors Vpu in the cellular membranes and a CT consisting of two putative α-helices separated by a conserved phosphorylation site (21). To understand which domain of Vpu interacts with hu-tetherin, we generated HEK 293 cells stably expressing KGC-tagged hu-tetherin (KGC-hu-tetherin) (Fig. 2D). Cells were transfected with plasmids encoding KGN-Vpu WT or mutants. We prepared KGN-tagged Vpu mutants by truncating its CT at residue 50 (Vpu1-50), replacing the TM region with a scrambled TM sequence (VpuRD), inserting an alanine at serine residues 52 and 56 in the cytoplasmic domain (Vpu2/6), or by inserting positively charged residues within the putative overlapping tyrosine- and dileucine-based sorting motifs with alanine (VpuR30A/K31A) (Fig. 1A) (12, 46, 58, 59). The levels of KGN-Vpu expression of these mutants were nearly equivalent (Fig. 2D, upper) and did not significantly alter KGC-hu-tetherin expression (Fig. 2D, lower). Our BiFC assay revealed that VpuRD interacted poorly with hu-tetherin, while Vpu1-50 displayed BiFC signals equivalent to those of WT Vpu (Fig. 2D, top columns), indicating that Vpu interacts with hu-tetherin through its TM domain. Moreover, VpuR30A/K31A displayed a modest decrease in BiFC signal. A previous study showed that the VpuR30A/K31A mutant displayed a partial (~40%) defect in its TGN localization and its efficient delivery to late endosomal degradation compartments (12). This indicates that the trafficking of Vpu to the TGN is important, to some extent, for hu-tetherin interaction. Our results confirm that Vpu and hu-tetherin interact with each other via their respective TM regions.

Mapping of the Vpu interaction domain in hu-tetherin TM. To reveal the Vpu-interacting amino acids in the TM region of tetherin, we next prepared plasmids encoding KGC-tagged hu-tetherin mutants with triple-alanine substitution in the TM region (Fig. 3A, top) and then transfected them into KGN-Vpu-expressing cells. Alanine is the substitution residue of choice, since it eliminates the side chain beyond the β-carbon and yet does not alter the main-chain conformation (as can glycine or proline), nor does it impose extreme electrostatic or steric effects (37). Levels of the cell surface expression of these mutants were nearly equivalent to or greater than that of WT hu-tetherin (Table 1). The levels of KGC expression detected by immunoblot analysis were equivalent to those of WT hu-tetherin (Fig. 3A, bottom), while LLL(22-24)AAA, IVI(34-36)AAA, LGV(37-39)AAA, and PLI(40-42)AAA showed clearly reduced BiFC signals compared to that of WT hu-tetherin (Fig. 3A). These data suggest that the residues covering 22 to 24 and 34 to 42 of hu-tetherin play a crucial role in the Vpu interaction. The reduction of Vpu binding capacity by the alteration of residues 22 to 24 in hu-tetherin might correspond to a previous observation that the deletion of 22L and 23L from hu-tetherin disrupts the interaction with Vpu (54).

To narrow down interacting amino acid residues within the 34 to 42 region of hu-tetherin, we next prepared single-alanine-substituted mutants (Fig. 3B, top). The levels of the cell surface protein expression of the mutants were equivalent to that of WT hu-tetherin (Table 1), and their electrophoretic mobilities were consistent with the expected sizes (Fig. 3B, bottom). Among the nine single-alanine-substituted mutants, I34A, L37A, and L41A mutations produced significantly reduced BiFC signals compared to hu-tetherin or its other mutants (Fig. 3B, right columns).

I34, L37, and L41 of hu-tetherin are involved in the determination of Vpu susceptibility. To examine whether the interaction between hu-tetherin and Vpu through I34, L37, and L41 residues plays a functional role in the determination of Vpu susceptibility, we tested these mutants for Vpu susceptibility and tetherin activity. HEK 293 cells were transfected with infectious WT HIV-1 DNA (pNL4-3) or its Vpu-deleted HIV-1 DNA (pNL4-3/Udel) together with WT hu-tetherin or its mutants. The amount of HIV-1 in the culture supernatants together with HIV-1 protein in cell extract was determined. Importantly, hu-tetherin mutants with I34A, L37A, P40A, and L41A mutations completely lost their Vpu susceptibility, while V35A, I36A, G38A, V39A, and I42A remained Vpu sensitive (Fig. 3C). To determine whether mutants that conferred resistance to antagonism by Vpu in virion release assays also conferred resistance to the downregulation of tetherin from the cell surface, we examined cell the surface expression of tetherin or its derivatives on these cells. In our results, the levels of the tetherin downregulation of I34A, L37A, and L41A mutants were similar to that of WT tetherin (Fig. 3D). On the other hand, only P40A displayed resistance to Vpu-induced downregulation. These results suggest that different mechanisms account for the loss of Vpu sensitivity in P40A and other mutants. Overall, these results provide direct evidence that I34, L37, and L41 of hu-tetherin are involved in the determination of Vpu susceptibility in addition to Vpu interaction. Interestingly, these amino acid residues are highly conserved among primate tetherins and are present not only in Vpu-sensitive but also in Vpu-insensitive tetherins (Fig. 3E, gray boxes 34, 37, and 41). This suggests that the presence of these residues alone is insufficient to render tetherin Vpu sensitive. Indeed, a previous report demonstrated that agm-tetherin interacted poorly with HIV-1 Vpu (54). Thus, we hypothesize that the difference of Vpu interaction efficiency between hu- and agm-tetherin is due to differences in secondary structure rather than the primary amino acid sequence of the TM domain. Furthermore, additional residues in human tetherin that are not conserved in monkey tetherins may contribute to Vpu sensitivity.

Acquisition of Vpu-interacting activity in agm-tetherin by the insertion of two amino acid residues and acquisition of Vpu susceptibility by a single amino acid mutation. To determine additional critical amino acid residues that affect Vpu interaction and susceptibility, we carried out both loss- and gain-of-function approaches using hu- or agm-tetherin. Human and chimpanzee tetherins contain a dileucine motif upstream of the Vpu binding domain that is absent from other

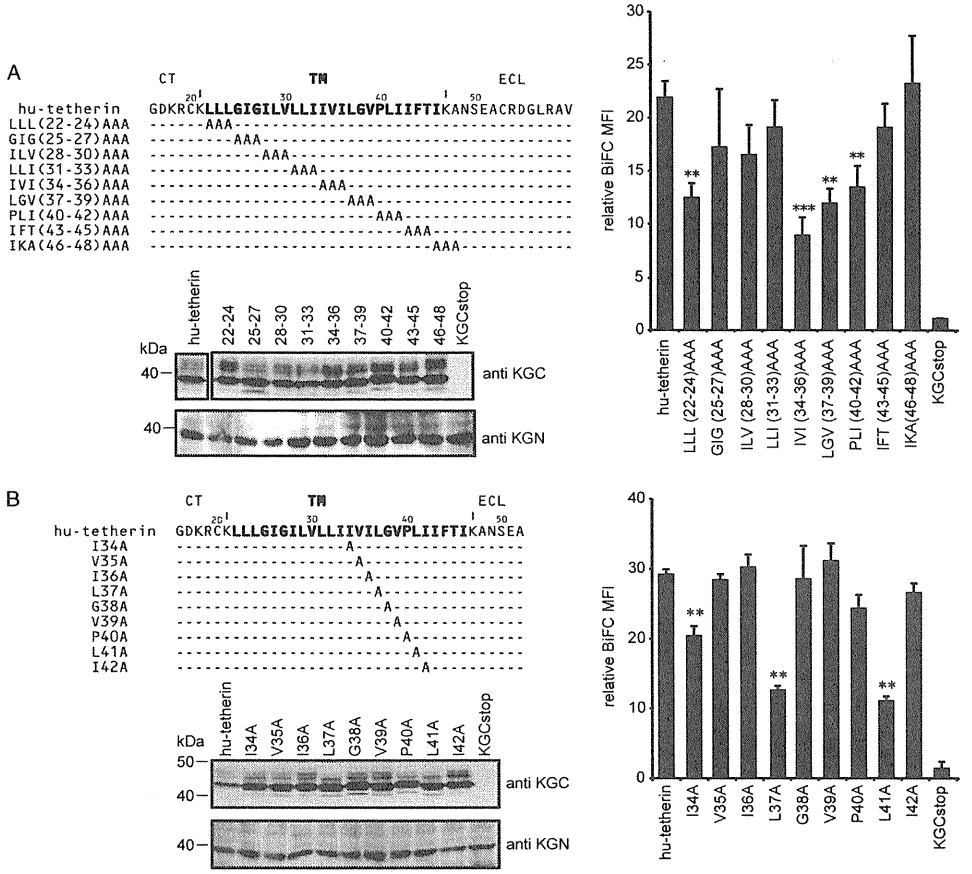

FIG. 3. Amino acid residues of hu-tetherin TM region required for Vpu interaction and counteraction. (A and B) BiFC assay of hu-tetherin TM mutants on Vpu interaction. Schematic diagram showing the amino acid alterations made in the C-terminal TM region of hu-tetherin. Identity is indicated by dashes. The KGN-Vpu-expressing cells were transfected with a series of KGC-hu-tetherin TM mutants and analyzed by flow cytometry as described in Materials and Methods. The protein expression of KGC-fused hu-tetherin and its mutants in cell lysates were detected using the indicated antibody. Relative MFI values are defined as the MFI of pKGN-Vpu-transfected or its mutant-transfected cells minus the MFI of untransfected cells, and results represent the means from three independent experiments plus standard deviations. (C) Tetherin activity and Vpu sensitivity of hu-tetherin TM mutants. HEK 293 cells were cotransfected with WT HIV-1 infectious DNA (pNL4-3) or its *vpu*-deleted DNA (pNL4-3/Udel) (1 μg) with or without (control) pKGC-hu-tetherin and its derivative expression plasmids (100 ng). The expression of HIV-1 ($Pr55^{Gag}$) in the cell lysates was detected using anti-p24 antibody. Results represent the means from more than three independent experiments. Statistical significance (Student's *t* test) is represented as $P < 0.05$ (**) and $P < 0.01$ (***) (A and B) or as numerical values (C). (D) Surface expression of tetherin and its mutants. HEK 293 cells were cotransfected with WT HIV-1 infectious DNA (pNL4-3) or its *vpu*-deleted DNA (pNL4-3/Udel) (1 μg) with or without (control) pKGC-hu-tetherin and its mutant expression plasmids (100 ng). The cell surface expression of tetherin was detected using anti-tetherin antibody. Statistical significance (Student's *t* test) is represented as $P < 0.05$ (*). (E) Amino acid alignment of seven primates and the mo-tetherin TM domain. Identity is indicated by dashes, and sequence gaps are indicated by an asterisk. Gray boxes indicate amino acid sequences corresponding to the mutants for which the BiFC signals were significantly decreased.

primate tetherins (Fig. 3E). The deletion of this motif (L22 and L23) in hu-tetherin clearly influenced its Vpu binding capacity (54). Another report demonstrated that a two-amino-acid deletion and a single-amino-acid substitution in the hu-tetherin TM (hu-delGI/T45I) can confer complete resistance to antagonism by Vpu (43). Hence, we focused on these two regions for the subsequent experiments (Fig. 4A). To confirm the lack of alteration of intracellular distribution of tetherin by deleting or inserting amino acid in its TM region, we examined the distribution of representative mutants (hu-delGI and agm-LL). The localizations of these mutants were very similar to that of hu-tetherin or agm-tetherin, respectively (Fig. 4B).

For the loss-of-function approach for hu-tetherin, we prepared KGC-tagged hu-delGI, hu-T45I, and hu-delGI/T45I tetherin mutants (Fig. 4A). Although the levels of KGC expression of these mutants were equivalent to that of WT hu-tetherin (Fig. 4C), hu-delGI and hu-delGI/T45I displayed significantly lower-level BiFC signals than WT hu-tetherin, while hu-T45I displayed a level of BiFC signals similar to that of WT hu-tetherin (Fig. 4C). Among these hu-tetherin mutants, hu-delGI/T45I showed the lowest interaction profile with Vpu. These data indicate that by itself T45 does not play a significant role in Vpu interaction; however, it exacerbates the effect of the GI deletion (G25 and I26). From tetherin activity and Vpu susceptibility assays, we confirmed that hu-delGI remained partially sensitive to Vpu (Fig. 4D) as previously described (43).

For the gain-of-function approach we prepared two KGC-tagged agm-tetherin mutants by inserting two leucine residues (agm-LL) or by combining the insertion of two leucines with a